VIRULENCE
2026, VOL. 17, NO. 1, 2677294
https://doi.org/10.1080/21505594.2026.2677294

Taylor & Francis
by informa

PATHOGEN GENOMICS

OPEN ACCESS Check for updates

Chromosome-level genome and transcriptome analysis of *Trichophyton verrucosum* reveals pathogenicity mechanisms and antifungal response

Muhammad Salman Tahir [a*], Xiaoping Ma [a*], Yu Gu [b*], Ruiguo Liu[a], Yingchong Liao[b], Xiangwen Zeng[a], Xing Zhao[a], Rongyan Luo[a], Bingying Li[a], Jianing Liu[a], Haiye Yang[a], Keying He[a], Sha Ye[b], Yan Tang[b], Hongrui Guo[a], Gang Ye[a], and Zhicai Zuo[a]

[a]Key Laboratory of Animal Disease and Human Health of Sichuan Province, College of Veterinary Medicine, Sichuan Agricultural University, Chengdu, China; [b]College of Life Sciences, Sichuan Agricultural University, Chengdu, China

ABSTRACT

Trichophyton verrucosum is a zoophilic dermatophyte and the primary cause of bovine dermatophytosis, a contagious and economically significant skin disease with zoonotic potential. Despite its importance, high-quality genomic and transcriptomic resources for this species remain scarce, limiting insights into its pathogenic mechanisms and antifungal responses. Here, we present a chromosome-level genome assembly of *T. verrucosum* OR056436.1, generated using single-molecule real-time (SMRT), Illumina paired-end and high-throughput chromosomal conformation capture (Hi-C) technologies, followed by comprehensive annotation and comparative analyses with six other fungal pathogens. Transcriptome profiling under itraconazole (ITR) and Xuanjing – Compound Chinese Herbal Spray (CCM) treatments revealed antifungal-responsive genes. The final 23.44 Mb genome comprises 7,936 protein-coding genes, with 4.98% repetitive sequences, and shows 98.8% completeness based on BUSCO analysis. Functional annotation identified 262 Kyoto Encyclopedia of Genes and Genomes pathways, 4,861 Eukaryotic Orthologous Groups proteins, 34 secondary metabolite biosynthetic gene clusters, 1,157 carbohydrate-active enzymes, 2,920 pathogen–host interaction genes, and 59 virulence factor genes. Comparative genomics identified 45,425 orthogroups including 393 core and 184 single-copy orthogroups, placing *T. verrucosum* closest to *Trichophyton rubrum*. Transcriptomic analysis highlighted differentially expressed genes enriched in amino acid metabolism, ABC transporters, drug metabolism, and stress response pathways. Notably, subtilisin-like proteases and LysM-domain proteins were significantly regulated under antifungal treatments. This integrative genomic-transcriptomic study provides the most complete *T. verrucosum* genome to date, identifies key genes involved in pathogenicity and antifungal adaptation, and offers valuable resources for diagnostics, therapeutic development, and improved strategies for bovine dermatophytosis.

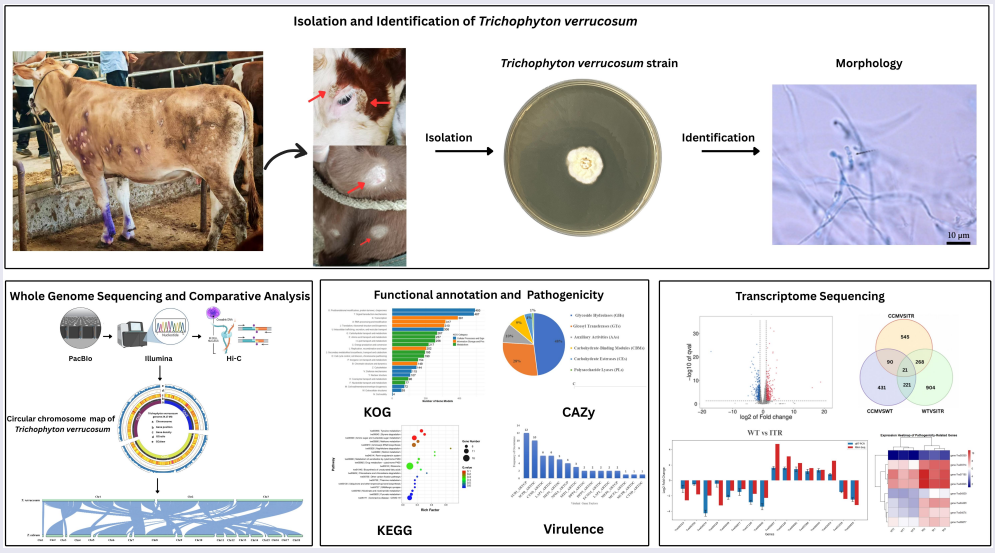

ARTICLE HISTORY

Received 26 September 2025
Revised 8 May 2026
Accepted 17 May 2026

KEYWORDS

Antifungal response; bovine dermatophytosis; comparative genomics; transcriptomics; *Trichophyton verrucosum*; virulence factors; Chromosome-level genome assembly

CONTACT Xiaoping Ma mxp886@sicau.edu.cn
*These authors contributed equally to this work and are co-first authors.
Supplemental data for this article can be accessed online at https://doi.org/10.1080/21505594.2026.2677294

Introduction

Dermatophyte infections, commonly known as tinea or ringworm, are a major public health concern worldwide. Dermatophytes are among the most prevalent pathogenic filamentous fungi, with global infection rates estimated at 20–25% [1]. Dermatophytosis is a contagious fungal infection caused by dermatophytes, a group of keratinophilic fungi that include anthropophilic, zoophilic, and geophilic species, of which only some are zoonotic [2,3]. These fungi infect keratinized tissues such as the skin, hair, and nails, leading to superficial infections [4]. They are widely distributed among humans, animals, and environmental reservoirs such as soil, and transmission occurs through direct contact or contaminated fomites [5]. Disease severity ranges from mild cutaneous infections to more severe or systemic conditions, depending on the host immune status [6]. Zoophilic dermatophytes predominantly infect animals but can also cause highly inflammatory infections in humans, and they are often carried asymptomatically in animal hair, facilitating transmission between animals and humans [7]. Dermatophytes primarily invade the stratum corneum of the epidermis and are major causative agents of animal dermatophytosis [8,9]. Among these, *Trichophyton mentagrophytes, Trichophyton verrucosum*, and *Microsporum canis* are the primary etiological agents of animal dermatophytosis [10,11]. Geophilic species such as *Nannizzia gypsea* (formerly *Microsporum gypseum*) may also be involved, whereas infections caused by anthropophilic species such as *T. rubrum* are rarely reported in animals [12,13]. Dermatophytes belong to the phylum *Ascomycota*, class *Eurotiomycetes*, order *Onygenales*, and family *Arthrodermataceae* [10,14]. Based on recent multilocus phylogenetic studies, this family comprises several genera, including *Trichophyton*, *Microsporum*, *Epidermophyton*, *Nannizzia*, *Arthroderma*, *Paraphyton*, and *Lophophyton* [10]. Host specificity varies among dermatophyte species; for example, *M. canis* is commonly associated with cats and dogs, *T. verrucosum* primarily infects cattle, and *T. mentagrophytes* infects a wide range of hosts, including rodents [15].

Trichophyton is a diverse genus comprising multiple recognized species, including anthropophilic, zoophilic, and geophilic members [10]. *T. verrucosum* is a zoophilic species that parasitizes keratinized tissues such as skin, hair, and nails in both animals and humans and is capable of degrading keratin, a key structural protein in these tissues [16]. In recent years, *T. verrucosum* has been increasingly associated with superficial infections in humans [17,18]. Infections are commonly acquired through direct or indirect contact with infected cattle or contaminated fomites, leading to inflammatory dermatophytosis and posing significant public health concerns [17]. *T. verrucosum* is the primary causative agent of bovine trichophytosis ("bovine ringworm") [19], a disease that is widely distributed worldwide and results in significant economic losses, including hide damage, weight loss, reduced meat and milk production, and treatment costs [20]. Understanding the genetic basis of the virulence of this pathogen is essential for improving treatment and control strategies [21].

The ability of fungi to recognize and adapt to host environments is critical for successful infection [22]. Pathogenic fungi detect host surface cues through cell wall components, monitor nutrient availability, and modify their cell walls to evade immune responses [23,24]. Adhesion to host tissues is mediated by carbohydrate-specific adhesins on the conidial surface and fibrillar projections that facilitate attachment to host cells [25]. Following adhesion, fungi establish infection by secreting enzymes such as lipases, phosphatases, and keratinolytic proteases that degrade host tissues [26]. The proteolytic breakdown of keratin releases oligopeptides and amino acids, including cysteine, which is metabolized by cysteine dioxygenase into sulfite to prevent cellular toxicity [27,28]. Proteases play a crucial role in dermatophyte pathogenicity; for example, the subtilisin protease SUB3 is involved in the attachment of *M. canis* to feline epidermis [29], while early infection stages of *T. rubrum* involve upregulation of genes encoding cell wall proteins such as Sowgp, highlighting their role in virulence [30]. Despite the increasing incidence of *T. verrucosum* infections, genomic insights into its pathogenic mechanisms remain limited, emphasizing the need for further investigation.

The advent of whole-genome sequencing has significantly advanced fungal biology. The sequencing of *Saccharomyces cerevisiae* in 1996 marked a milestone in fungal genomics and provided a foundation for understanding eukaryotic microorganisms [31]. In dermatophytes, *Trichophyton benhamiae* and *T. verrucosum* were among the first species to be sequenced, with approximately 97% of their ~22.5 Mb genomes assembled [32]. Subsequently, additional dermatophyte genomes, including *T. rubrum, Trichophyton tonsurans, Trichophyton equinum, M. canis*, and *N. gypsea*, were reported [33]. Comparative genomic analyses have identified gene families associated with pathogenicity, such as proteases, kinases, secondary metabolites, and LysM-

domain-containing proteins, which may help mask fungal cell wall components and evade host immune responses [33,34]. Advances in sequencing technologies, particularly third-generation platforms such as PacBio, enable long-read sequencing and near-complete genome assembly, although with higher error rates compared to second-generation methods [35]. Hybrid sequencing approaches combining long- and short-read data improve assembly accuracy and facilitate comprehensive genomic analyses, including gene annotation, virulence factor identification, and host – pathogen interaction [36]. For *T. verrucosum*, such integrative approaches provide valuable insights into its adaptation and pathogenicity.

Transcriptome sequencing (RNA-seq) enables high-throughput and accurate quantification of gene expression, allowing comparative analysis across different conditions [37–39]. In fungal research, RNA-seq has been widely used to identify differentially expressed genes in response to antifungal treatments, providing insights into drug mechanisms and resistance pathways [40–44]. For example, transcriptomic analysis has been used to elucidate the inhibitory effects of ketoconazole on *M. canis* [44], while studies on *T. rubrum* have revealed transcriptional responses to antifungal agents such as acriflavine [45]. These approaches have significantly improved our understanding of molecular mechanisms underlying fungal pathogenicity and drug responses [46,47]. Identification of key genes and pathways involved in host – fungus interactions provides potential targets for the development of novel antifungal therapies [48,49].

Despite the increasing prevalence and zoonotic potential of *T. verrucosum*, genomic and transcriptomic resources for this species remain limited. Compared to well-characterized dermatophytes such as *T. rubrum* and *M. canis*, the molecular basis of *T. verrucosum* pathogenicity and antifungal resistance is still poorly understood. To address this gap, we generated a chromosome-level genome assembly of *T. verrucosum* using SMRT, Illumina, and Hi-C sequencing technologies. Genes associated with virulence were functionally annotated, and comparative genomic analyses were conducted with other pathogenic fungi, including *T. rubrum, M. canis, Candida albicans, N. gypsea, Aspergillus fumigatus*, and *T. tonsurans*. Furthermore, transcriptomic profiling under itraconazole (ITR) and Xuanjing – Compound Chinese Herbal Spray (CCM) treatments identified differentially expressed genes involved in stress response, virulence regulation, and potential antifungal resistance. These findings provide a comprehensive genomic and transcriptomic framework for *T. verrucosum*, offering valuable insights for diagnosis, antifungal drug development, and disease control strategies.

Materials and methods

Isolation, culture, morphological and biochemical characterization of Trichophyton verrucosum

Trichophyton verrucosum was isolated from skin scrapings and dander of *Bos taurus* (beef cattle) showing clinical signs of dermatophytosis. A total of five cattle aged 6–10 months, all exhibiting alopecic lesions consistent with dermatophytosis, were included in this study. The animals showed localized skin lesions without other systemic clinical signs and had not received antifungal treatment prior to sampling. Information regarding dermatophytosis in in-contact humans was not available. Verbal consent was obtained from the farm owner during the diagnostic sampling process for the participation of the cattle in this study.

The fungal isolate was maintained at the College of Veterinary Medicine Laboratory, Sichuan Agricultural University (Chengdu, China). Small amounts of dander from the samples were inoculated onto DTM (dermatophyte test medium; Qingdao Hope Bio-Technology Co., Ltd.) by applying tiny particles of dander onto the agar surface with sterilized forceps using the three-point inoculation technique. The inoculated plates were incubated at 28°C and monitored daily for colony development. Visible fungal growth appeared after 7–9 days of incubation, while well-developed colonies were observed within 10–15 days. Emerging colonies were subsequently subcultured onto Sabouraud dextrose agar (SDA) and SDA supplemented with malt extract (SDAM) to obtain pure cultures. The SDAM medium provided a relatively nutrient-rich environment that may influence colony morphology, pigmentation, vegetative hyphal growth, and sporulation patterns. No other fungal contaminants were observed, and pure cultures were successfully obtained following subculturing.

To assess temperature-dependent growth characteristics, cultures were incubated at both 28°C and 37°C for 15–21 days. Macroscopic colony morphology was evaluated based on growth rate, colony texture, surface appearance, elevation, and pigmentation under both temperature conditions. Microscopic characteristics were examined by preparing mounts stained with lactophenol cotton blue. Slides were observed under light microscopy to evaluate hyphal structure, limited conidial formation, and diagnostic microscopic features

such as chains of chlamydospores and antler-like hyphae.

Biochemical characterization was performed to further support species identification. Proteolytic activity was assessed on bromocresol purple casein milk inositol (BPC) agar after 7 days of incubation, where the presence of a clear hydrolysis zone indicated a positive reaction. Urease activity was determined using Christensen's urea agar after 3–5 days of incubation, with a color change from yellow to pink indicating urease production. Morphological and biochemical characteristics were interpreted in conjunction with molecular identification to ensure accurate species confirmation.

DNA extraction and ITS sequencing

Genomic DNA was extracted using the fungal genomic DNA Rapid Extraction Kit (Sangon Biotech, Shanghai, Co., Ltd) following the manufacturer's instructions. The internal transcribed spacer (ITS) region was amplified with primers ITS1 (5"-TCCGTAGGTGAACCTGCGG-3") and ITS4 (5"-TCCTCCGCTTA TTGATATGC-3") in a 25 µL polymerase chain reaction (PCR) containing ddH_2O (8.5 µL), forward and reverse primers (1 µL each), DNA template (2 µL), and 12.5 µL Premix Taq (Ex Taq version2.0). A pan-dermatophyte-specific PCR assay was not performed; instead, molecular identification was based on ITS sequencing.

PCR conditions were an initial denaturation at 94°C for 10 min, followed by 30 rounds of denaturation at 94°C for 30 s, annealing at 55°C for 30 s, extension at 72°C for 1 min and 10 s, and finally a 72°C extension for 5 min. PCR products were visualized on 1.2% agarose gel containing Gold View dye (Accurate Biotechnology, Hunan, Co., Ltd)at 120 V for 20 min to check for target bands. The target band-containing amplification products were sent to Chengdu Shenggong Biotechnology Co., Ltd. for sequencing. Blast comparison with NCBI GenBank confirmed strain identity as *T. verrucosum* OR056436.1 and was kept in storage at the China Centre for Type Culture Collection. The phylogenetic tree of strain *T. verrucosum* OR056436.1 was constructed using Mega 12 (version 12).

PacBio-based genome sequencing and Assembly

For whole-genome sequencing, the quality and quantity of extracted genomic DNA were accessed using a NanoDrop 2000 spectrophotometer (NanoDrop Technologies, Wilmington, DE, USA), a Qubit 3.0 Fluorometer (NanoDrop Technologies, Carlsbad, DE, USA), and 0.8% agarose gel electrophoresis. The SMRTbell library was constructed using the SMRTbell Express Template Prep Kit 2.0 (Pacific Biosciences). Genomic DNA (~15 µg) was mechanically snipped to fragments (15 kb) using a Covaris g-TUBE, followed by size selection using the BluePippin system (Sage Science). The quality and number of size-selected libraries were assessed using the Femto Pulse system and a Qubit fluorometer (Life Technologies, Carlsbad, CA, USA), respectively. The library was loaded with an on-plate concentration of 120 pM using diffusion loading. SMRT sequencing was performed using a single 8 M SMRT Cell on the Sequel II System with Sequel II Sequencing Kit, 1800-minute movies by Frasergen Bioinformatics Co., Ltd. (Wuhan, China).

Initial assembly was performed using HiFiasm (v0.16.1) [50] with default parameters, and the gfa tools (https://github.com/lh3/gfatools) were used to transform sequence graphs to FASTA format, followed by assessment with Benchmarking Universal Single-Copy Orthologue (BUSCO, v5.2.2) [51].

Hi-C sequencing and chromosome assembly

Hi-C libraries were constructed following the protocol described by [52]. Briefly, *T. verrucosum* conidia were treated with 1% formaldehyde (v/v) to maintain DNA structure. Then, the cross-linked DNA was digested with restriction endonuclease MboI (New England Biolabs Inc., Ipswich, MA) to generate sticky ends. To reverse DNA cross-linking, the DNA fragments were ligated using 50 U T4 DNA ligase (NEB) and then digested with proteinase K (Thermo Fisher, Waltham, MA). The DNA was then purified and arbitrarily sheared into fragments of 300–500 bp. Biotin-labeled DNA was extracted by using streptavidin-interceded pull-down and PCR amplification, and Hi-C libraries were quantitated and sequenced on the Illumina Novaseq platform (San Diego, CA, USA) or MGI seq platform (BGI, China).

Trimmomatic (v0.40) [53] was used to clean high-quality paired-end reads, and all filtered reads were matched to contigs using a juicer (v3, https://github.com/aidenlab/juicer) to measure the contact frequency [54]. By using default parameters, 3ddna (v180922) [55] was used for misjoin correction ($-r_2$). The orientated scaffolds were utilized to create the interaction matrices to analyze and manually repair with Juicebox assembly tools (v1.11.08) [54]. Completeness was assessed by employing the fungi_odb10 gene set with BUSCO (v5.2.2) [51].

Repeat and non-coding RNA annotation

We combined homology-based and de novo methods to identify the repeat sequences in the genome. A homology-based approach to homologous sequence prediction was based on the known Repbase repetitive sequence database (http://www.girinst.org/repbase) [56]. We used RepeatMasker software (open-4.0.9) [57], RepeatProtein Mask software [57], and an ab initio approach [58] to predict and identify known repeat-like sequences. We built an ab initio repeat sequence library using RepeatModeler software (http://www.repeatmasker.org/RepeatModeler/) [57], and identified LTR retrotransposons using LTR-FINDER software (v1.0.7) [59]. RepeatMasker software [57] was used to search for similar transposable elements (TE) in the known Repbase TE library [56], and de novo repeat library. Tandem repeats were detected using Tandem Repeat Finder (TRF) with parameters (2 7 7 80 10 50 2000) [60]. Sequence similarity searches were performed with an E-value threshold of ≤1e − 5. TE copy numbers were estimated from the output of RepeatMasker Sequence similarity searches were performed using an E-value threshold of ≤1e − 5. TE copy numbers were estimated based on repeat annotation outputs generated by RepeatMasker [57].

We used tRNAscan-SE (v2.0.9) [61], with default parameters to identify tRNA genes, which are adaptor molecules that bridge the genetic code in mRNA with the amino acid code in proteins. Potential pseudogenes were filtered out using tRNAscan-SE's internal scoring criteria. Ribosomal RNA (rRNA) sequences were predicted using RNAmmer (v1.2) [62]. Small nuclear RNAs (snRNAs) and microRNAs (miRNAs) were identified using Infernal (v1.1.2) [63] against the Rfam database (v14.6) [64], with default parameters. Additionally, repeat sequences, including tandem repeats and high-copy tRNA families, were annotated using Tandem Repeat Finder (TRF) and RepeatMasker-based approaches to minimize interference from repetitive regions and ensure that the tRNA predictions are not biased by repetitive elements.

Prediction of genetic structure was accomplished using the union of three methods: (1) homology-based prediction, which involves the comparison of genome sequence of the related species with the reference genome using Tblastn (v2.11.0+) [65]. Then, the aligned sequences and their analogous proteins were cleaned and transmitted to the Exonerate (v2.4.0) for accurate alignment [66]. (2) transcriptome-based prediction, gene structures predicted by MAKER were refined by incorporating RNA-seq data through PASA (v2.4.1) [67]. PASA significantly improved the accuracy of gene annotations by adding untranslated regions (UTRs) and refining alternative splicing events, ensuring that the gene models were consistent with transcript evidence. (3) De novo prediction utilizing Augustus [68], Glimmer HMM [69], and Genscan [70] for the prediction of gene structure using preexisting probabilistic model characteristics to predict gene features, such as exon-intron boundaries and UTRs. The integration of these three approaches through MAKER (v3.01.03) [71], resulted in a non-redundant and more comprehensive gene set. Further refinements were made using PASA [67], in conjunction with transcriptomic data to ensure high accuracy in the gene structure predictions.

Gene functions were annotated by lining up protein sequences to many databases such as SwissProt (https://web.expasy.org/docs/swiss-prot_guideline.html) [72], the National Center for Biotechnology Information (NCBI) Non-Redundant (NR) (ftp://ftp.ncbi.nlm.nih.gov/blast/db/FASTA/nr.gz), Gene Ontology (GO) (http://geneontology.org/page/go-database) [73], Kyoto Encyclopedia of Genes and Genomes database (KEGG) (http://www.genome.jp/kegg/) [74], InterPro (http://www.ebi.ac.uk/interpro/) [75], and TrEMBL (https://www.ebi.ac.uk/uniprot/) [72].

KEGG pathway analysis was conducted using the KEGG Automatic Annotation Server (KAAS) [76]. Functional gene classification was performed using the EuKaryotic Orthologous Groups (KOG) database [77]. Gene clusters for secondary metabolites were anticipated using the antiSMASH fungal version. The program identified many biosynthetic gene clusters, including non-ribosomal peptide synthetases (NRPS), polyketide synthases (PKS), terpenes (TC), and hybrids. The clusters demonstrate the potential of *T. verrucosum* to synthesize secondary metabolites with varying variety [78].

Pathogenicity gene annotation

We used a variety of databases to annotate genes linked to pathogenicity in the *T. verrucosum* genome. CAZymes (Carbohydrate-Active Enzymes Database) (http://www.cazy.org) [79] was employed to annotate carbohydrate-active enzymes which included the enzyme families to catalyze carbohydrate breakdown, modification, and biosynthesis. They were divided into six main groups, which were Glycoside Hydrolases (GHs), Glycosyl Transferases (GTs), Auxiliary Activities (AAs), Carbohydrate Esterases (CEs), Polysaccharide Lyases (PLs), and Carbohydrate-Binding Modules (CBMs). We utilized the dbCAN-

HMMdb-V7 version of dbCAN2 for the annotation of carbohydrate-related enzymes [80]. The Pathogen–Host Interaction Database (PHI-base) (http://www.phi-base.org) was used to analyze pathogen–host interaction (PHIs) genes [81]. Additionally, database of fungal virulence factors (DFVF) (http://sysbio.unl.edu/DFVF/) [82] was employed to reveal the distinct virulent genes in the genome.

Comparative genomics

Comparative genomic analysis was performed to explore the pathogenicity/resistance mechanism of *T. verrucosum*. The whole genomic protein sequences of *T. rubrum*, *M. canis*, *Candida albicans*, *M. gypseum, Aspergillus fumigatus*, and *T. tonsurans* etc. were downloaded from NCBI (https://www.ncbi.nlm.nih.gov/genome/), and the orthologous protein sequences in the genome were analyzed using OrthoFinder [83]. The aligning of single-copy core orthologous proteins was performed using MAFFT [84], followed by species phylogenesis inference using the maximum probability method in IQ-TREE [85]. The One Step MCScanX module in TBtools (v1.1047) was used to investigate genome-wide replication events across species [86].

Genome-based taxonomic Validation

To confirm the taxonomic identity of the isolate at the whole-genome level, Average Nucleotide Identity (ANI) analysis was performed using FastANI. This method employs a Mashmap-based, alignment-free approach, where genome sequences are fragmented into 3 kb segments and compared in an all-versus-all manner to estimate genomic similarity.

In addition to ANI analysis, k-mer – based similarity analysis was conducted using sourmash (v4.0). Genomic signatures were generated using a k-mer size of 31 and a scaling factor of 1000 (MinHash approach), allowing for the estimation of Jaccard similarity between genomes based on shared k-mer content. This approach enables a comparison of genomes at the k-mer level, providing a more detailed view of genomic relationships.

Reference genomes of closely related dermatophyte species, including *T. rubrum* and *T. mentagrophytes*, were used for comparative analysis. The results from both the ANI and Mash distance analyses showed clear clustering of the isolate with *T. verrucosum* and distinct separation from both *T. rubrum* and *T. mentagrophytes*, confirming the taxonomic identity of the isolate as *T. verrucosum*.

Antifungal susceptibility testing

Antifungal susceptibility testing was performed using the broth microdilution method in accordance with the Clinical and Laboratory Standards Institute (CLSI) guidelines for filamentous fungi. Antifungal agents, including ketoconazole (KTZ), itraconazole (ITR), terbinafine (TBF), amphotericin B (AMB), fluconazole (FCA), 5-fluorocytosine (5-FC), and ciclopirox olamine (CPX), were prepared as stock solutions at a concentration of 512 μg/mL.

The fungal spore suspension was prepared from fresh cultures and adjusted to a final concentration of 1×10^6 CFU/mL. Minimum inhibitory concentrations (MICs) were determined using a two-fold serial dilution method in sterile 96-well microtiter plates. The MIC was defined as the lowest concentration of antifungal agent that inhibited visible fungal growth after incubation.

Antifungal treatment and transcriptomic analysis

For transcriptome profiling, the isolate was cultured on SDAM (50 mL), Itraconazole medicine (ITR) (0.5 μg/mL), and Xuanjing – Compound Chinese Herbal Spray (CCM) (75 μg/mL) (Design Biotechnology, Co., Ltd). Two groups were used: wild type (WT) group cultured on SDAM; treatment groups exposed to ITR and CCM. Each treatment condition was performed in triplicate, with each replicate processed and sequenced individually to ensure biological reproducibility. Samples were randomized across sequencing lanes to mitigate potential batch effects. Itraconazole was selected for transcriptomic analysis based on its observed sensitivity against the isolate and its clinical relevance in dermatophytosis treatment.

SDAM medium was prepared by dissolving 1.6 g glucose, 1 g peptone, 1.5 g agar and 0.6 g malt extracted in distilled water to a final volume of 50 mL. Itraconazole was first dissolved in dimethyl sulfoxide (DMSO) to prepare a stock solution at a concentration of 12,800 μg/mL by dissolving 51.2 mg in 4 mL of DMSO. The working solution was prepared by diluting the stock solution in Sabouraud dextrose agar medium to obtain a final concentration of approximately 0.5 μg/mL.

Sophora flavescens, Densefruit Pittany Rootbark, *Phellodendron chinense*, *Cortex Pseudolaricis*, *Cnidium monnieri*, and other herbs were ground, sieved, and extracted with 70% ethanol (1:12) after soaking and ultrasonication to prepare CCM in the laboratory. The extract was concentrated to 1 g/mL and stored in 2%

dimethyl sulfoxide (DMSO). CCM stock solution was prepared by dissolving 0.375 mL in 49.6 mL SDAM to achieve a final concentration of 75 µg/mL. The strains were incubated at 28°C and colony growth was observed and monitored daily for the duration of 15–21 days. After 14th day incubation, the samples from all the cultures were scraped into 2 mL cryotube, immediately frozen in liquid nitrogen and stored at −80°C for RNA extraction.

Transcriptome sequencing and analysis

The two sets of samples: WT and treatment group obtained in the previous period were sent to Lianchuan Biotechnology Co., Ltd. (Qiantang, Hangzhou) for transcriptome sequencing. Total RNA was isolated with TRIzol reagent (Thermo Fisher) following the manufacturer's protocol and quantified using an RNA 6000 Nano LabChip Kit and Bioanalyzer 2100 (Agilent, CA, USA, 5067–1511). mRNA was purified from 5 µg of total RNA using Dynabeads Oligo (dT) (Thermo Fisher, CA, USA) for library preparation. Short mRNA fragments were created using the Magnesium RNA Fragmentation Module (NEB, cat. e6150, USA). Fragmented RNA was reverse-transcribed into cDNA using SuperScript™ II (Invitrogen), and U-labeled second-strand DNA was synthesized with DNA polymerase I, RNase H (NEB), and dUTP (Thermo Fisher). According to vendor's recommended protocol, paired-end sequencing (2 × 150 bp, PE150) was performed on an Illumina NovaSeq™ 6000 platform (LC-Biotechnology Co., Ltd., Hangzhou, China). The reads generated for each library were filtered by using Cutadapt (v1.9, https://cutadapt.readthedocs.io/en/stable/) [87]. HISAT (v2.2.1, https://daehwankimlab.github.io/hisat2/) was used to align high-quality reads to the *T. verrucosum* de novo genome [87,88]. Mapped reads were assembled with StringTie (v2.1.6, http://ccb.jhu.edu/software/stringtie/) [89], and merged using gffcompare (v0.9.8, http://ccb.jhu.edu/software/stringtie/gffcompare.shtml) to generate a comprehensive transcriptome. Transcript expression levels were estimated as fragments per kilobase of transcript per million mapped reads (FPKM) using StringTie and Ballgown (http://www.bioconductor.org/packages/release/bioc/html/ballgown.html) [90].

Differential expression and functional enrichment

Gene differential expression analysis was performed using DESeq2 to compare two groups, with *T. verrucosum* cultured on SDAM medium as the control. The genes with the parameter of false discovery rate (FDR) below 0.05 and absolute fold change ≥2 were considered differentially expressed genes (DEGs) [91]. Gene enrichment analysis (GO) and pathway enrichment analysis (KEGG) were performed by using Gene Ontology database (http://www.geneontology.org/) and KEGG database (https://www.kegg.jp/kegg/) for the functional annotation of *T. verrucosum* [73,92]. Gene set enrichment analysis (GSEA, v4.1.0) [93] was performed to determine whether genes associated with specific GO terms and KEGG pathways were significantly different between the two groups [94].

Quantitative real-time RT-PCR (qRT-PCR) Validation

qRT-PCR was performed to validate the expression of 16 selected differentially expressed genes (DEGs) to ensure the reliability of transcriptome sequencing data. Specific primers for qRT-PCR were designed using Primer 6.0 software (Supplementary Table S1).

Total RNA was extracted from the samples, and first-strand cDNA was synthesized from 2 µL of DNase-treated RNA using a commercial kit from Accurate Biotechnology (Hunan, China). The qPCR was carried out using the SYBR Green Premix Pro Taq HS Kit (Accurate Biotechnology) on a Rocgene real-time PCR system. Each 20 µL reaction mixture contained 10 µL of 2× SYBR Green mix, 0.4 µL of each 10 µM primer, 1 µL cDNA, and RNase-free water. The cycling conditions were as follows: 95°C for 30 s, followed by 40 cycles of 95°C for 5 s, 60°C for 30 s, and 65°C for 5 s. GAPDH was used as the reference gene, and reactions were performed in triplicate. Gene expression levels were quantified using the 2^−ΔΔCt method [93].

Results

Clinical features, morphological and biochemical characterization of Trichophyton verrucosum

The infected cattle exhibited typical clinical signs of dermatophytosis, including circular alopecic lesions with scaling and crust formation on the skin (Figure 1(A)). Colony morphology of the isolate was evaluated on SDAM under different temperature conditions. At 28°C (Figure 1(B)), colonies were slow-growing, compact, centrally elevated, and restricted, forming dense button-like structures with smooth and well-defined margins. Mature colonies exhibited slight cream-to-pale yellow pigmentation in the central region. At 37°C (Figure 1(C)), colonies showed comparatively increased radial expansion, appearing larger with a more diffuse and less compact peripheral zone while

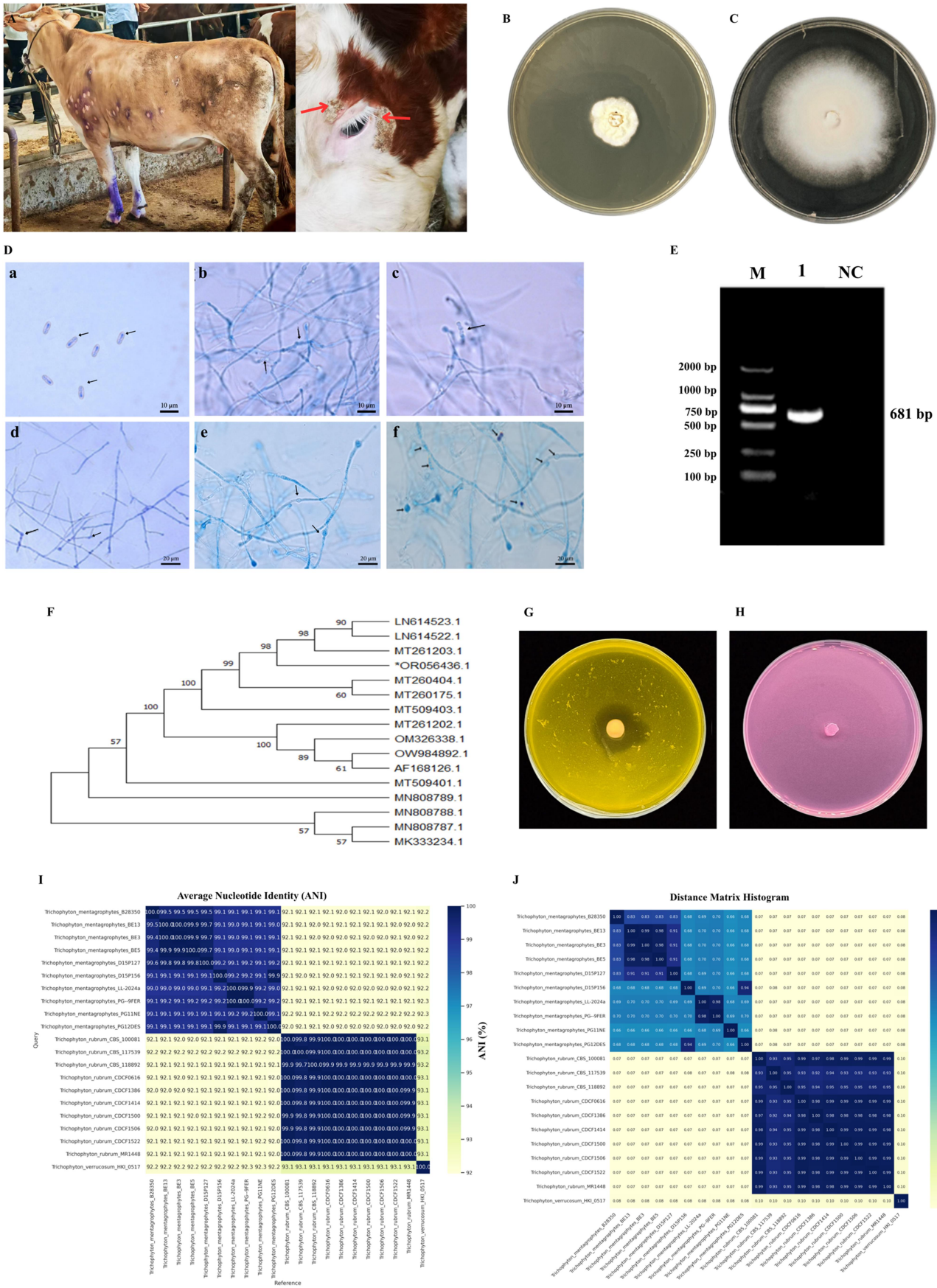

Figure 1. Clinical features, morphological, molecular, and genomic characterization of *Trichophyton verrucosum*. (a) Clinical presentation of dermatophytosis in cattle showing circular alopecic lesions with scaling and crusting.(B – C) colony morphology on

retaining a slightly raised central morphology. These findings demonstrate temperature-dependent growth characteristics consistent with the known biology of *Trichophyton verrucosum*. Variations in colony morphology and pigmentation may occur depending on strain characteristics, culture medium composition, incubation conditions, and duration of growth.

Microscopic examination using lactophenol cotton blue staining revealed septate hyaline hyphae, abundant chains of thick-walled chlamydospores, sparse conidial elements occasionally observed, and branched antler-like (favic chandelier) hyphae (Figure 1(D)). Chains of chlamydospores represented the predominant microscopic feature observed under the present culture conditions. These findings are consistent with the established morphological variability reported for *T. verrucosum*.

Biochemical characterization confirmed enzymatic activities associated with pathogenicity. The isolate exhibited positive proteolytic activity, as evidenced by a clear hydrolysis zone on bromocresol purple casein milk inositol (BPC) medium after 7 days of incubation (Figure 1(G)). Urease activity was also positive, indicated by a color change from yellow to pink on Christensen's urea agar after 3–5 days of incubation (Figure 1(H)). These findings, together with morphological characteristics, are consistent with classical descriptions of *T. verrucosum* and support reliable species identification.

Molecular identification based on ITS sequencing

PCR amplification of the ITS region produced a clear single band of approximately 681 bp (Figure 1(E)), confirming successful amplification of fungal DNA. All samples showed identical banding patterns, indicating reproducibility and genetic consistency of the isolates. The amplified ITS products were sequenced, and BLAST analysis against the NCBI GenBank database showed 99–100% similarity with *T. verrucosum* (accession no. OR056436.1). Phylogenetic analysis demonstrated that the isolate clustered with reference *T. verrucosum* strains with high bootstrap support (Figure 1(F)), confirming its identity at the species level.

Genome assembly and quality assessment

PacBio sequencing generated 7,950,199,200 bp of subreads (332.9× coverage) from a single Sequel II SMRT cell. Based on HiFi read statistics, 5.51 Gb of sequence data were obtained, corresponding to a total genome size of 5,513,614,564 bp and 230.9× coverage. A total of 308,142 reads were generated, with an average read length of 17,893 bp, an N50 of 18,034 bp, and a GC content of 46.5% (Supplementary Figure S1A).

The initial HiFiasm assembly produced 74 contigs with a total length of 26,374,647 bp (26.37 Mb) and a contig N50 of 5,797,948 bp (5.79 Mb). K-mer analysis (k = 17) (k depth = 271) estimated a genome size of 24.17 Mb, with low heterozygosity (0.01%) and repeat content of 8.08%, indicating a highly homozygous genome.

After filtering low-quality sequences from the MGISEQ-2000 platform, 7,716,051,900 bp (7.71 Gb) of clean reads (230.9× coverage) were obtained, with 97.01% mapping to the initial PacBio assembly. Following Hi-C scaffolding, the draft assembly size was 23.88 Mb with an anchoring rate of 98.16%. Following Hi-C–based correction, the final assembly size was 23.44 Mb (23,441,077 bp), comprising 14 contigs, of which four were anchored into three chromosomes. Chromosome 1 consisted of two contigs, while chromosomes 2 and 3 each consisted of a single contig, with the remaining contigs unanchored. The final assembly achieved a contig N50 of 6.08 Mb and a scaffold N50 of 7.02 Mb (Table 1). The final genome size (23.44 Mb) is consistent with the k-mer estimate (24.17 Mb) and falls within the reported range for dermatophytes (22.5–24.17 Mb). The larger initial assembly size (26.37 Mb) likely reflects redundant or heterozygous contigs that were removed during Hi-C

Sabouraud dextrose agar supplemented with malt extract (SDAM): (b) slow-growing, compact, centrally elevated button-like colony with restricted radial expansion and slight cream-to-pale yellow pigmentation at 28 °C; (c) larger colony with increased radial expansion and diffuse peripheral growth at 37 °C.(D) Microscopic characteristics observed using lactophenol cotton blue staining: (a) sparse conidial elements, (b) conidial structures, (c) characteristic chains of thick-walled chlamydospores, (d) septate hyphae, (e – f) antler-like (favic chandelier) hyphae.(E) PCR amplification of the ITS region showing a ~ 681 bp band confirming fungal DNA amplification.(F) Phylogenetic tree based on ITS sequences showing clustering of the isolate with reference *T. verrucosum* strains.(G – H) biochemical characterization: (g) proteolytic activity on BPC medium; (h) urease activity on Christensen's urea agar.(I) Heatmap of Average nucleotide identity (ANI) showing genomic similarity among *T. verrucosum*, *T. rubrum*, and *T. mentagrophytes*.(J) Mash distance matrix representing k-mer – based genomic distance among the three dermatophyte species.

Table 1. Summary of genome assembly and annotation features of *Trichophyton verrucosum*..

Feature	*Trichophyton verrucosum*
Assembly	
Chromosomes	3
Largest chromosome length (bp)	10,334,313
Smallest chromosome length (bp)	6,084,903
Number of contigs	14
Final assembly size (bp)	23,441,077
Contig N50 (bp)	6,084,903
Scaffold N50 (bp)	7,022,361
GC content (%)	51.155
BGI reads mapping rate (%)	95.75
BGI reads coverage (%)	99.98
HiFi reads mapping rate (%)	97.01
HiFi reads coverage (%)	99.88
BUSCO completeness (%)	98.8
Complete (%)	98.3
Duplicated (%)	0.3
Fragmented (%)	0.3
Missing (%)	0.9
QV	52.1781
Gene Structure Information	
Protein-coding genes in the chromosomes	7,936
Average gene length (bp)	1,481
Average CDS length (bp)	1,165
Average exons per gene	2.8
Average exon length (bp)	441
Average intron length (bp)	152
Non-coding RNA Information	
rRNAs (copy)	131
tRNAs (copy)	84
snRNA (copy)	27
CD-box (copy)	18
HACA-box (copy)	5
Splicing RNA (copy)	4
scaRNA (copy)	0

scaffolding and curation. The low heterozygosity (0.01%) and low BUSCO duplication rate (0.5%) support a well-collapsed genome assembly without evidence of uncollapsed haplotigs.

Genome completeness was assessed using BUSCO v5.2.2 with the fungi_odb10 dataset. A total of 98.8% complete BUSCOs were identified, including 98.3% single-copy and 0.5% duplicated, with 0.3% fragmented and 0.9% missing, indicating high completeness (Table 1).

To validate the chromosome-level assembly, a Hi-C contact map was generated (Supplementary Figure S1C). The heatmap showed strong intra-chromosomal interactions along the diagonal and three distinct interaction blocks corresponding to the three chromosomes, with weak inter-chromosomal signals. No obvious off-diagonal signals were observed after correction with 3D-DNA and JuiceBox. The high read mapping rate (99.16%) and anchoring efficiency (98.16%) further support assembly accuracy. Alignment against the NCBI NT database showed that 50.16% of reads matched *T. verrucosum*, while the remaining reads aligned with closely related dermatophyte species, indicating minimal contamination and high data reliability.

Repeats and non-coding RNAs

Analysis of non-coding RNA identified 84 tRNA genes, 131 rRNA. A total of 27 snRNAs were identified, comprising 18 C/D-box, 5 H/ACA-box, and 4 spliceosomal RNAs (Table 1), which are key regulators of gene expression and cellular processes.

Various types of transposable elements (TE) have been identified in *T. verrucosum*, which exhibits notable discrepancies in both abundance and diversity. Despite having a relatively low transposable element (TE) content, *T. verrucosum* contained two major classes of retrotransposons: long interspersed nuclear elements (LINEs) and long terminal repeats (LTRs), with a minimal presence of short interspersed nuclear elements (SINEs). Combined results from both homology-based and de novo detection methods, after redundancy removal, indicated that repeat sequences accounted for approximately 4.98% (1,189,375 bp) of the genome, including 3.64% transposable elements (TEs). Among TEs, DNA transposons were most abundant (2.37%), followed by LTRs (0.73%) and LINEs (0.53%), while SINEs were rare (0.01%) (Table 2).

Gene structure and functional annotation

Using the MAKER and PASA pipelines, a total of 7,936 protein-coding genes were predicted, with an average gene length of 1,481 bp and a mean exon count of 2.8 (Table 1). Functional annotations across several key databases identified 7,539 genes (95.00%), leaving 397 unannotated genes (5.00%) (Supplementary Table S1). The highest annotation rate was achieved by the NR database with 7,535 genes (94.95%), followed closely by TrEMBL (7,507 genes, 94.59%). KEGG_ALL annotated 7,265 genes (91.54%), while GO annotated 5,668 genes (71.42%), and InterPro annotated 5,534 genes (69.73%). The KEGG_KO subset annotated 3,420 genes (43.09%), and SwissProt annotated 5,036 genes (63.46%).

A total of 3,420 genes were annotated across all seven databases, while 1,616 genes were annotated in

Table 2. Identification of transposable element sequences in *Trichophyton verrucosum*.

Features	Combined TE Length (bp)	Combined TE in the Genome (%)
DNA Transposons	565,421	2.37
LTR	174,473	0.73
LINE	125,787	0.53
SINE	2121	0.01
Other	0	0.00
Unknown	29,166	0.12
Total TE	869,807	3.64

six databases. Additionally, 1,597 genes were consistently annotated by NR, TrEMBL, and KEGG_ALL, while 242 genes were jointly annotated by NR and TrEMBL, and 28 genes were uniquely annotated by NR (Supplementary Figure S3).

The gene structure predictions were supported by PASA's transcript evidence, with 99.88% of the predicted genes refined by PASA annotations, and 0.11% being supported only by ab initio predictions. PASA introduced significant annotation edits, including the addition of UTRs and the refinement of alternative splicing events, ensuring higher accuracy and alignment with transcript evidence.

KEGG pathway analysis of *T. verrucosum* identified 262 functional metabolic pathways, with a high concentration of genes in metabolic processes (Figure 2 (A)). The most represented categories included carbohydrate metabolism (418 genes), amino acid metabolism (345), lipid metabolism (300), metabolism of cofactors and vitamins (265), nucleotide metabolism (260), glycan biosynthesis and metabolism (173), and energy metabolism (117). Key amino acid pathways were highlighted and encompassed tryptophan metabolism (118), lysine degradation (55), and tyrosine metabolism (48). Among the 418 genes involved in carbohydrate metabolism, the most represented pathways were amino sugar and nucleotide sugar metabolism (90 genes), starch and sucrose metabolism (81), and butanoate metabolism (54). Many xenobiotic degradation pathways (201 genes), including those for benzoate (49), gamma-hexachlorocyclohexane, and caprolactam (24) were found in *T. verrucosum*. Furthermore, 183 genes were linked to pathways that produce secondary metabolites, such as anthocyanins, carotenoids, and flavonoids (Supplementary Table S3A).

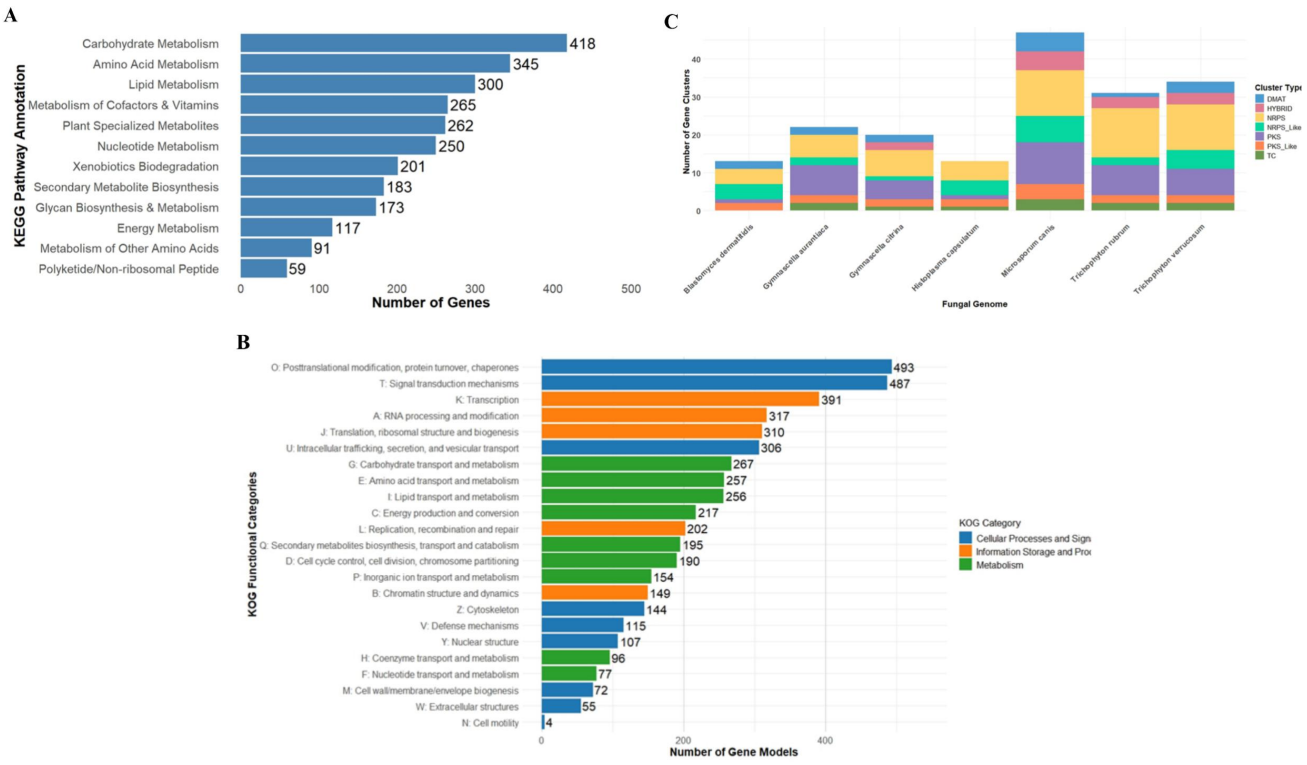

Figure 2. Functional annotation and secondary metabolite biosynthetic potential of *Trichophyton verrucosum* Genome.(A) Kyoto Encyclopedia of genes and genomes (KEGG) pathway annotation. This panel displays the main KEGG pathways with their names and the total number of genes associated with each pathway. The x-axis indicates the number of genes (up to 500), while the y-axis lists the KEGG pathway in ascending order based on gene count. (B) EuKaryotic orthologous groups (KOG) classification. This panel shows the functional categorization of proteins in *T. verrucosum* based on KOG grouping. The x-axis represents the number of gene models, whereas the y-axis displays the KOG functional categories. Three primary KOG categories were listed with their functional id and total number of genes: cellular processes and signaling (1783), Information storage and processing (1369), and metabolism (1709), respectively. (c) Secondary metabolic gene clusters in seven fungal genomes including *T. verrucosum*. This panel compares the number of secondary metabolites biosynthetic gene clusters across seven fungal genomes. The x-axis indicates the fungal species, and the y-axis shows the number of gene clusters. *M. canis* exhibits the highest number (47), followed by *T. verrucosum* (34), and *T. rubrum* (31). The type of each cluster was listed: DMAT (dimethylallyl tryptophan synthase), hybrid clusters, NRPS (non-ribosomal peptide synthetases), NRPS-like, pks (polyketide synthases), PKS-like, and terpenes (TC).

The KOG database annotated about 4,861 genes according to functional categories based on protein functions (Figure 2(B)). Cellular processes and signaling were linked to 1,783 genes, prominently featuring posttranslational modification, protein turnover, and chaperones (493 genes), signal transduction mechanisms (487 genes), and intracellular trafficking, secretion and vesicular transport (306 genes). Functions of genetic information processing were delineated by 1,369 genes, primarily related to transcription (391 genes), RNA processing (317 genes), and translation (310 genes). The metabolism comprised 1,709 genes, with carbohydrate metabolism (267 genes), amino acid metabolism (257 genes), and lipid metabolism (256 genes) representing the primary functional groups exhibiting considerable enrichment (Supplementary Table S3B). The findings demonstrate the sophisticated regulatory, metabolic, and structural genomic capacities, which relate to its capacity for adaptability and pathogenicity of *T. verrucosum*.

Genomic analysis of *T. verrucosum* identified 34 secondary metabolite biosynthetic gene clusters (BGCs) with diverse class composition: 3 DMAT (dimethylallyl tryptophan synthase), 3 hybrid clusters, 12 NRPS (nonribosomal peptide synthetases), 5 NRPS-like, 7 PKS (polyketide synthases), 2 PKS-like, and 2 terpenes (TC) (Figure 2(C)). In comparison to other fungal genomes, *T. verrucosum* has a relatively high capacity for secondary metabolite production, however it is inferior to *M. canis* (47 BGCs) and superior to *T. rubrum* (31 BGCs) (Supplementary Table S3C). The substantial presence of NRPS and PKS clusters suggests the capacity to produce a diverse array of bioactive metabolites that may enhance the pathogenicity and environmental adaptability of *T. verrucosum* and serve as a source of novel metabolites.

Pathogenicity-associated genes

A significant number of pathogenicity-associated genes were found to understand the pathogenic mechanism of *T. verrucosum*. Carbohydrate-active enzymes (CAZymes) may influence the life cycle and pathogenicity of dermatophytes, potentially revealing novel molecular targets for therapeutic and diagnostic applications. The CAZy annotation of the *T. verrucosum* genome identified 1,157 carbohydrate-active enzyme genes, including 562 (48%) glycoside hydrolases (GHs), 326 (28%) glycosyl transferases (GTs), 116 (10%) auxiliary activity enzymes (AAs), 100 (9%) carbohydrate-binding modules (CBMs), 44 (4%) carbohydrate esterases (CEs), and 9 (1%) polysaccharide lyases (PLs) (Figure 3(A)).

PHI-base analysis identified 2,920 pathogen–host interaction (PHI)-related genes, including 1,427 associated with reduced virulence, 918 with unaffected pathogenicity, 248 with loss of pathogenicity, 113 lethal, 166 with increased virulence, and 17 linked to chemical drug interactions (Figure 3(B)).

Furthermore, the DFVF database provided insights into distinct virulence-associated gene families within the *T. verrucosum* genome. Analysis identified 15 unique virulence gene families, exhibiting varying frequencies of occurrence and diverse functional roles (Figure 3(C)). Among these, SUB1_ARTGP (subtilisin-like protease) was the most frequent, detected 12 times, followed by SCPB_ARTOC (secreted cysteine protease), which appeared 10 times. These gene families are involved in protein degradation, particularly keratin, which is crucial for pathogenicity in dermatophytes. Other notable virulence factors identified included CTSD_ARTOC, LAPI_ARTOC (lysosomal aspartic proteases), each appearing 6 times, followed by MEPI_ARTOC (metalloprotease), detected 5 times. Additional virulence factors such as NPIIA_ARTGP, SED1_ARTOC, DPP4_ARTOC, DPP5_ARTOC, ECM14_ARTOC, LAP2_ARTOC, MEP6_ARTOC, MCPA_ARTOC, MCPB_ARTOC, and CTSD_ARTOC were identified at lower frequencies (1–4 occurrences). These virulence factors are integral to the pathogenic mechanisms of *T. verrucosum* and may provide critical insights for future therapeutic strategies (Table 3).

A comprehensive analysis of pathogenicity-related genes was performed using the CAZy, PHI-base, and DFVF databases to explore the virulent mechanisms of *T. verrucosum*. The Venn diagram (Figure 3(D)) summarizes the overlap and unique contributions of these databases, identifying 437 genes unique to CAZy, 695 genes shared between CAZy and PHI-base, 1,879 genes unique to PHI-base, and 16 genes unique to DFVF. This visualization highlights both core virulence factors shared between species and species-specific genes that may drive pathogenicity in dermatophytes.

Comparative genomics

Comparative genomic analysis promotes the understanding of evolutionary links and gene function across many species by identifying gene sequences and their arrangement, classifying gene families, and evaluating genome collinearity. OrthoFinder grouped 54,808 genes from seven species into 45,425 orthogroups, with 82.9%

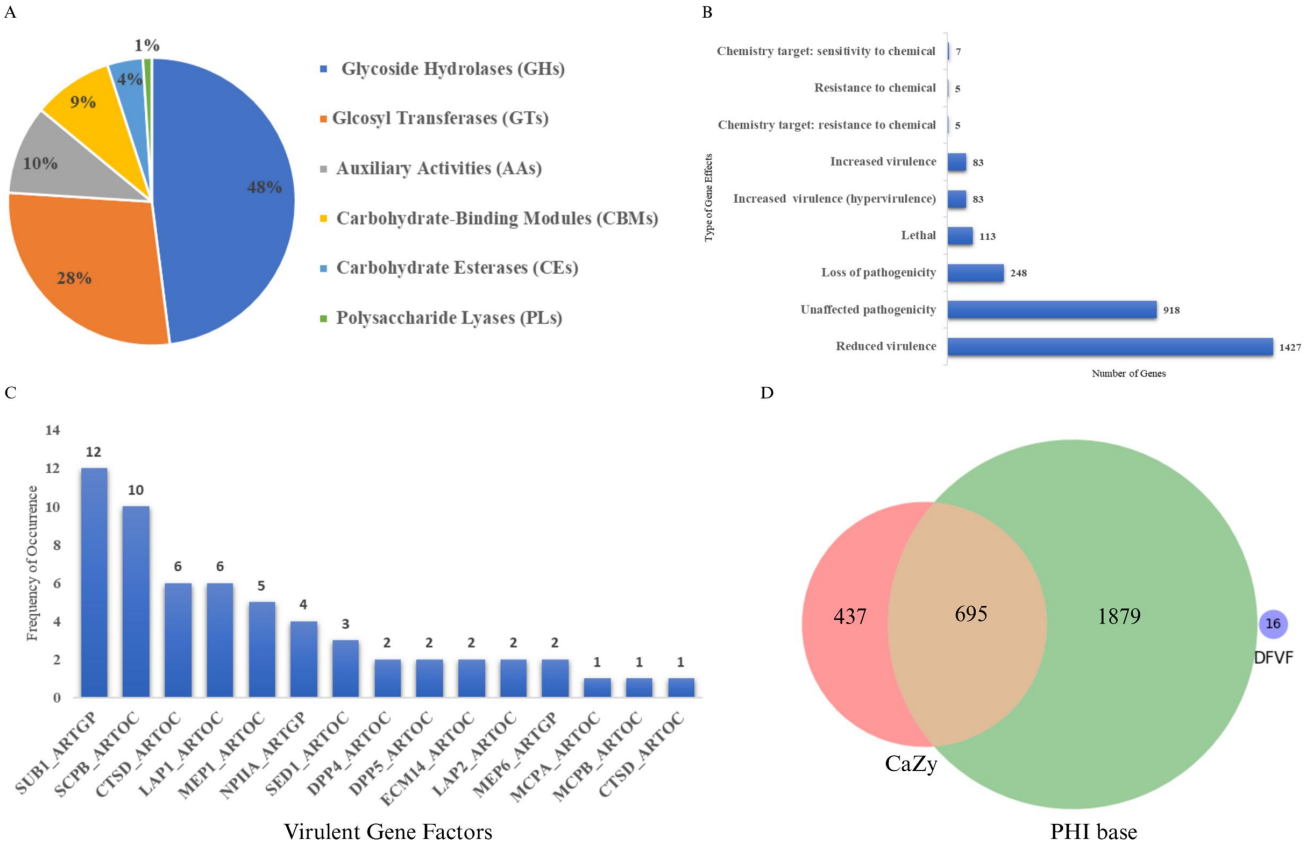

Figure 3. Summary of annotations for pathogenicity-related genes in *Trichophyton verrucosum*. (A) Carbohydrate-active enzymes (CAZys). Pie chart showing the distribution of different CAZyme families involved in host cell wall degradation. The categories include Glycoside Hydrolases (GHs, 48%), glycosyl transferases (GTs, 28%), auxiliary activities (AAs, 10%), carbohydrate-binding modules (CBMs, 9%), carbohydrate esterases (CEs, 4%), and polysaccharide lyases (PLs, 1%).(B) Pathogen-host interaction (PHIs) annotations. Bar chart illustrating the number of genes associated with different pathogenicity-related effects. The most prevalent categories include genes linked to reduced virulence (1,427), unaffected pathogenicity (918), and loss of pathogenicity (248), followed by lethal (113), increased virulence (166), and chemical resistance (17) categories. (C) Virulence-associated genes from the database of fungal virulence factors (DFVF). Bar chart showing the frequency of occurrence of specific virulence factors. The most frequently identified genes include SUB1_ARTGP (12), SCPB_ARTOC (10), CTSD_ARTOC (6), LAP1_ARTOC (6), and others involved in fungal virulence. (D) Venn diagram showing the overlap of pathogenicity-related genes from the CaZy, PHI-base, and DFVF databases. The diagram highlights core virulence factors shared across species and species-specific genes unique to *T. verrucosum*. 437 genes are unique to CaZy, 695 genes are shared between CaZy and PHI-base, 1879 genes are unique to PHI-base, and 16 genes are unique to DFVF.

of genes assigned to orthogroups containing two or more genes (G50 = 6). The largest orthogroup comprised 3,557 genes (O50 = 3,557). Comparative investigations have found key orthogroups shared among dermatophytes, as well as species-specific genes that may promote host adaptation. A total of 393 core orthogroups were shared across all species, including 184 composed of single-copy genes (Figure 4(A)). These core orthogroups represent a conserved genomic backbone across dermatophytes, indicating strong evolutionary conservation of essential functions. The presence of 184 single-copy orthologs further supports their evolutionary stability and phylogenetic relevance, while variation in orthogroup composition may contribute to differences in host adaptation and pathogenicity.

The total number of orthogroups and species-specific orthogroups was 45,425 and 103, respectively, and the gene distribution across species is shown in Figure 4(A). Single copy orthogroups were used to construct phylogenetic trees, revealing that *T. verrucosum* is most closely related to *T. rubrum*, followed by *M. gypseum* and *M. canis* (Figure 4(B)). Significant collinearity was observed between the genomes of *T. verrucosum* and *T. rubrum*, supported by 6,942 shared orthogroups. Collinearity block analysis further illustrates the chromosomal relationships between these two species. *T. verrucosum* contains

Table 3. Virulence genes, gene counts, families and functions in *Trichophyton verrucosum*.

Gene ID	Number	Family	Function
SUB1_ARTGP	12	Peptidase S8	Secreted subtilisin-like serine protease with keratinolytic activity that contributes to pathogenicity.
SCPB_ARTOC	10	Peptidase S10	Extracellular serine carboxypeptidase that contributes to pathogenicity.
CTSD_ARTOC	6	Peptidase A1	Secreted aspartic-type endopeptidase which is secreted and contributes to virulence.
LAP1_ARTOC	6	Peptidase M28	Extracellular aminopeptidase which contributes to pathogenicity.
MEP1_ARTOC	5	Peptidase M36	Secreted metalloproteinase probably acting as a virulence factor.
NPIIA_ARTGP	4	Peptidase M35	Secreted metalloproteinase that allows assimilation of proteinaceous substrates. Shows high activities on basic nuclear substrates such as histone and protamine. May be involved in virulence.
SED1_ARTOC	3	Peptidase S53	Secreted tripeptidyl-peptidase which degrades proteins at acidic pHs and is involved in virulence.
DPP4_ARTOC	2	Peptidase S9B	Extracellular dipeptidyl-peptidase which removes N- terminal dipeptides sequentially from polypeptides having unsubstituted N-terminal provided that the penultimate residue is proline. Contributes to pathogenicity.
DPP5_ARTOC	2	Peptidase S9B	Extracellular dipeptidyl-peptidase which removes N- terminal dipeptides sequentially from polypeptides having unsubstituted N-terminal. Contributes to pathogenicity.
ECM14_ARTOC	2	Peptidase M14	Probable carboxypeptidase that may be involved in cell wall organization and biogenesis.
LAP2_ARTOC	2	Peptidase M28	Extracellular aminopeptidase that releases a wide variety of amino acids from natural peptides and contributes to pathogenicity.
MEP6_ARTGP	2	Peptidase M43B	Secreted metalloproteinase that allows assimilation of proteinaceous substrates. Plays a pivotal role as a pathogenicity determinant during infections and contributes to the ability of the pathogen to persist within the mammalian host.
MCPA_ARTOC	1	Peptidase M14	Extracellular metalloprotease that contributes to pathogenicity.
MCPB_ARTOC	1	Peptidase M14	Extracellular metalloprotease that contributes to pathogenicity.
CTSD_ARTOC	1	Peptidase A1	Secreted aspartic-type endopeptidase which is secreted and contributes to virulence.

three chromosomes (Chr1, Chr2, and Chr3), each showing collinearity with chromosomes of *T. rubrum*. Specifically, Chr1 aligns with *T. rubrum* chromosomes 1–6, while chromosomes 13–18 also exhibit collinearity with Chr1 (Figure 4(C)). The high collinearity between *T. verrucosum* and *T. rubrum* underscores their close evolutionary relationship and suggests shared pathogenic mechanisms among dermatophytes.

Genome-based confirmation of species identity

Average Nucleotide Identity (ANI) analysis demonstrated that *Trichophyton verrucosum* showed the highest genomic similarity with *T. rubrum* (94.27%), followed by *T. mentagrophytes* (93.42%) (Figure 1(I)). While these values are below the commonly accepted species threshold of ~95%, they confirm that the isolate is a distinct species, separate from both *T. rubrum* and *T. mentagrophytes*.

To further evaluate genomic relatedness, k-mer –based Mash distance analysis was performed (Figure 1(J)). This analysis revealed variation in genomic similarity patterns compared to ANI, reflecting differences in genome composition among the species. While ANI indicated closer nucleotide-level similarity between *T. verrucosum* and *T. rubrum*, Mash analysis revealed distinct clustering patterns, highlighting the evolutionary divergence and genome-level variation among these dermatophytes. The Mash distance analysis reinforces the finding that *T. verrucosum* is genetically distinct from both *T. rubrum* and *T. mentagrophytes*, despite sharing a certain level of genomic similarity.

Antifungal susceptibility profile of Trichophyton verrucosum

Antifungal susceptibility testing revealed that strain OR056436.1 was highly sensitive to ketoconazole and itraconazole, with low MIC values (1–2 μg/mL and 0.5–1 μg/mL, respectively). Moderate susceptibility was observed for 5-fluorocytosine (MIC: 32 μg/mL). In contrast, the isolate exhibited high MIC values for terbinafine (64 μg/mL), amphotericin B (64 μg/mL), fluconazole (256 μg/mL), and ciclopirox olamine (16–-64 μg/mL), indicating resistance to these agents. Based on this susceptibility profile, itraconazole was selected for subsequent transcriptomic analysis. Detailed MIC values and interpretations are presented in Supplementary Table S4.

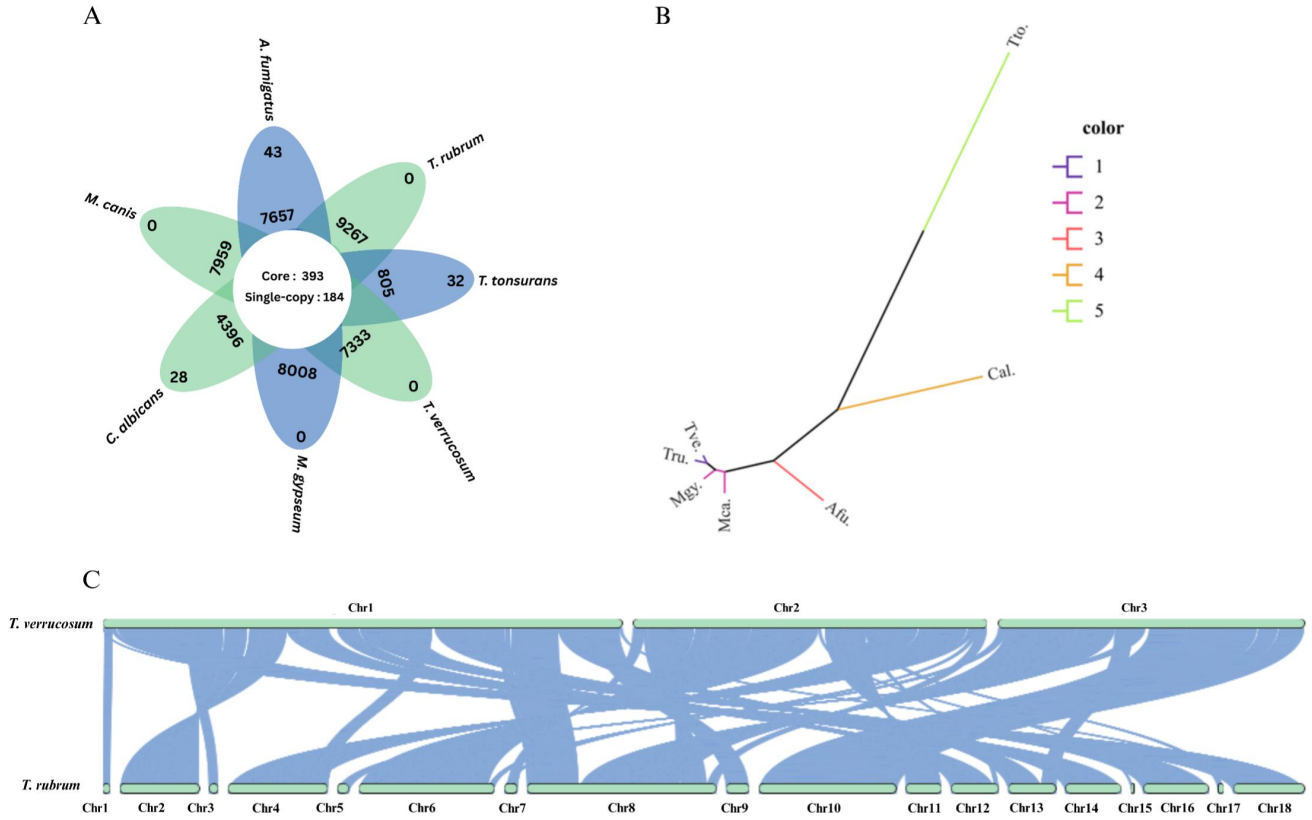

Figure 4. Comparative genomic analysis of animal pathogens associated with cattle bovine disease (CBD).(A) Summary of orthogroups across seven species. A flower plot showing the distribution of orthogroups among seven fungal pathogens. The central core contains 393 shared orthogroups, including 184 single-copy orthogroups. The inner rings represent the total number of genes within orthogroups for each species, while the outermost segments indicate the number of species-specific genes unique to each species (B) Phylogenetic tree analysis based on single-copy core orthogroups. This panel depicts the evolutionary relationship between *Trichophyton verrucosum* and six other CBD-associated pathogens, inferred from single-copy core orthogroups.(C) Collinearity between *T. verrucosum* and *Trichophyton rubrum*. this panel displays the synthetic relationship between the genomes of *T. verrucosum* (chromosome 1–3) and *T. rubrum* (chromosome 1–18), highlighting conserved genomic blocks and chromosomal rearrangements.

Transcriptional profiling of Trichophyton verrucosum

Transcriptional profiling of *T. verrucosum* was performed by culturing the isolate under three conditions: SDAM medium (control), ITR (treatment) and CCM (treatment). High-throughput RNA sequencing generated an average of 42,938,807 raw reads and 41,369,622 clean reads across all samples. Clean reads for the individual groups were 43,832,042 for WT (control), 42,198,780 for ITR (treatment), and 38,078,044 for CCM (treatment) (Supplementary Table S5).

Sequencing quality was high and consistent across groups, with the alignment rates for each group being similar: 97.74% for WT, 97.97% for ITR, and 97.49% for CCM, indicating uniform alignment performance. Moreover, most reads were aligned to exonic regions, with percentages ranging from 71.49% to 78.42% (Supplementary Table S6). Additionally, a substantial proportion of paired-end reads mapped successfully, with rates ranging from 90.12% to 94.12%, further confirming the high integrity of the sequencing data. These findings demonstrate that alignment rates and read quality were uniform across the control and treatment groups, ensuring reliable data for downstream transcriptional analysis.

Analysis of differentially expressed genes (DEGs)

Differential gene expression analysis of WT, ITR, and CCM samples was conducted using the FPKM method to quantify transcript levels in *T. verrucosum* strains. Based on FPKM values, correlations between all

samples were calculated. Pearson's correlation coefficients approaching 1 indicated strong similarity between samples. The three biological replicates of the same *T. verrucosum* strain exhibited the highest similarity, with most of the correlation coefficients generally exceeding 0.6. WT vs. ITR or CCM showed generally lower *R*-values (~0.2–0.5), indicating distinct gene expression patterns. Principal component analysis (PCA) was conducted to evaluate the distribution patterns of WT, ITR, and CCM samples (Supplementary Figure S4).

Comparison was performed between CCM vs. ITR, CCM vs. WT, and WT vs. ITR and observed a differential expression of genes among all three comparison groups. A total of 1,880 were significantly expressed, of which 936 were significantly up-regulated and 944 were significantly down-regulated (Figure 5(A-C)). Total differentially expressed genes were 545 in group CCM vs. ITR, of which 334 were significantly up regulated and 211 were significantly downregulated. CCM vs. ITR had 431 differentially expressed genes, from which 135 genes were up-regulated, and 296 genes were down-regulated significantly. In the WT vs. ITR comparison, 904 genes were differentially expressed, with 467 significantly upregulated and 437 downregulated. A Venn diagram revealed 21 DEGs shared across all three comparison groups (Figure 5(D)).

Functional enrichment analysis of DEGs

GO and KEGG enrichment analyses were performed to elucidate the biological functions of DEGs across all three comparisons (Figure 6). GO enrichment analysis revealed that DEGs were distributed across three categories: biological process, cellular component, and molecular function. Within biological processes, the most enriched terms were proteolysis (GO:0006508), methylation (GO:0032259), amino acid transmembrane transport (GO:0003333), and

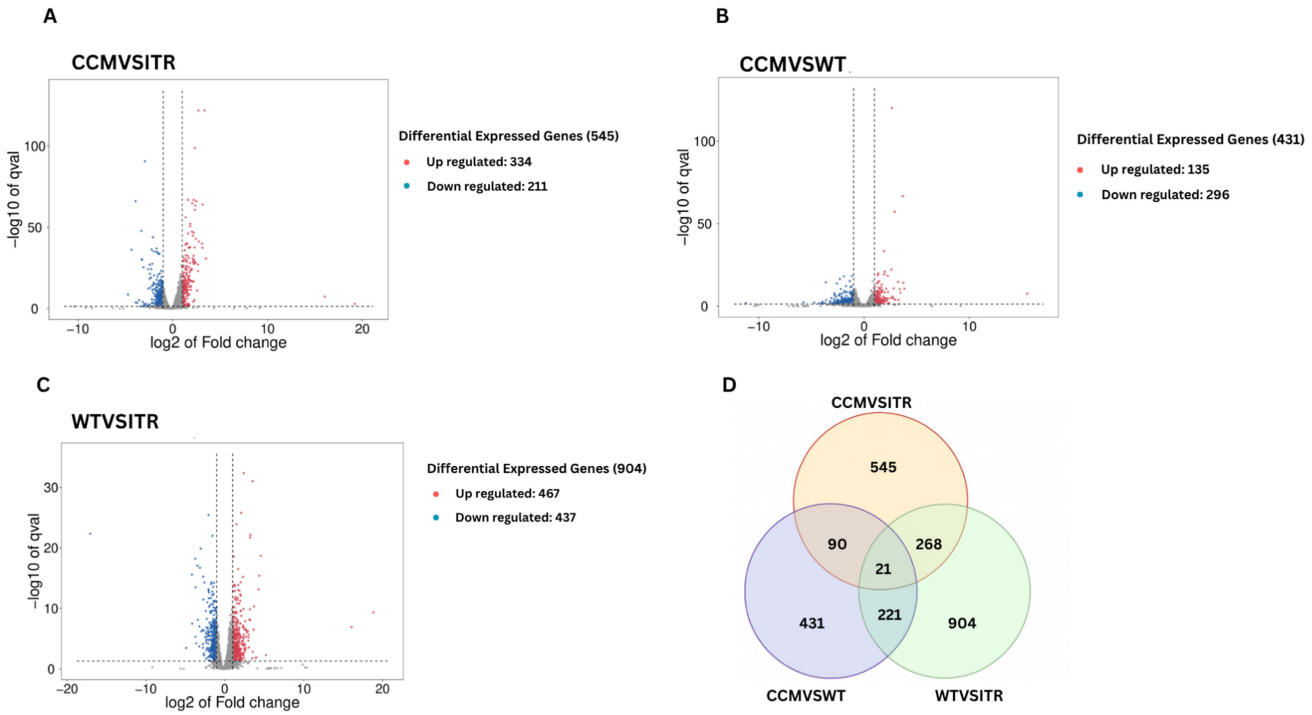

Figure 5. Differential gene expression analysis across three pairwise comparisons using volcano plots and a Venn diagram. (A).CCM vs. ITR comparison. A total of 545 differentially expressed genes (DEGs) were identified, including 334 upregulated (red) and 211 downregulated (blue) genes. The x-axis shows the $\log_2$ Fold change in gene expression, while the y-axis indicates the -$\log_{10}$ of the adjusted q-value, highlighting significantly regulated genes. (B). CCM vs. WT comparison. A total of 431 DEGs were observed, with 135 genes upregulated and 296 genes downregulated. This indicates a predominance of gene suppression in CCM-treated group compared to the wild type.(C). WT vs. ITR comparison. This comparison revealed the highest number of DEGs (904), with 467 genes upregulated and 437 downregulated, reflecting extensive transcriptomic alterations in response to itraconazole treatment. (D).Venn diagram of DEGs across all comparisons. The Venn diagram illustrates the overlap of DEGs among the three pairwise comparisons. A total of 21 genes were commonly regulated across all three groups. Additional subsets include shared and unique DEGs such as 90 genes overlapping between CCM vs. ITR and CCM vs. WT.

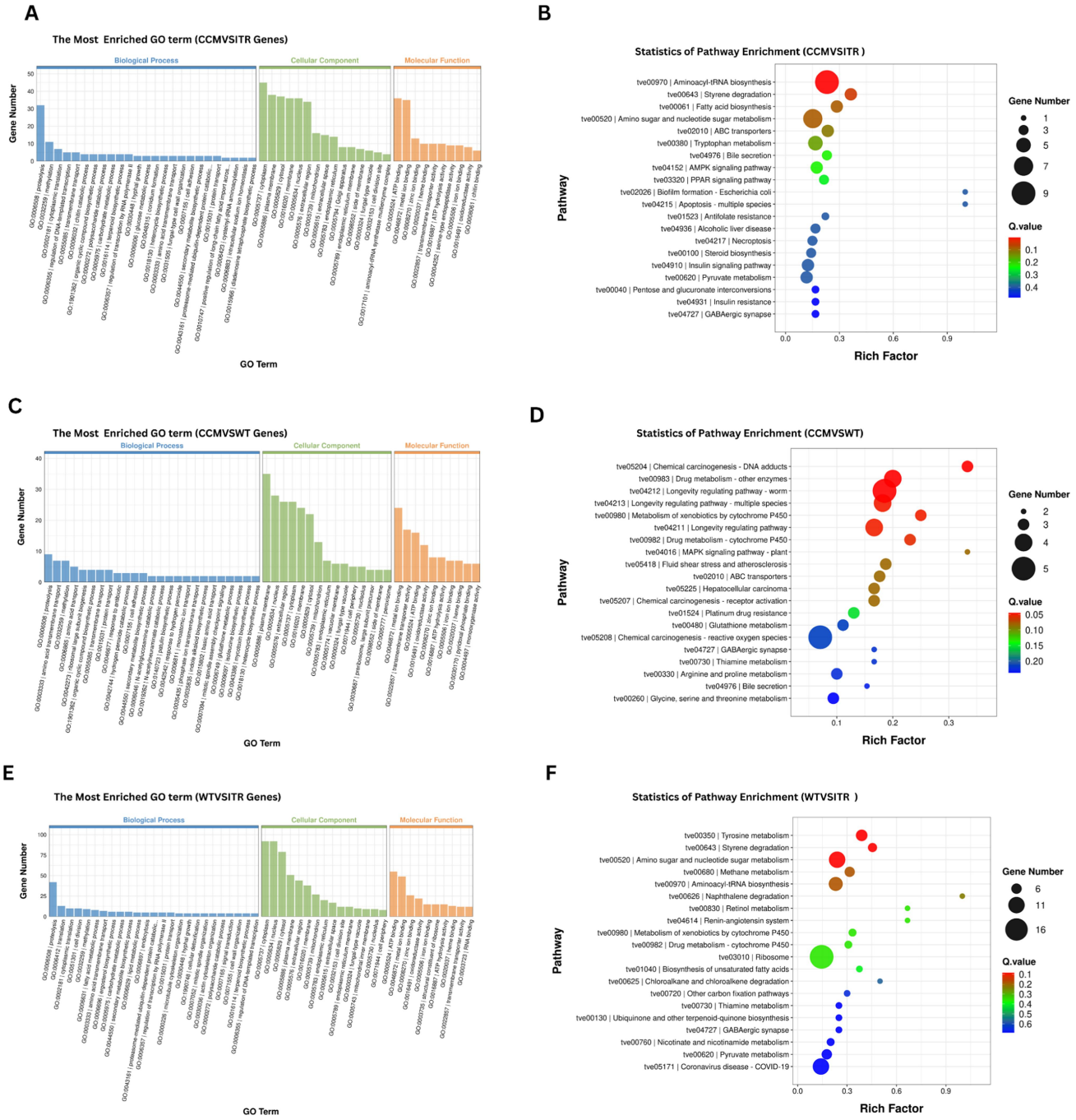

Figure 6. Functional annotation and pathway enrichment analysis of differentially expressed genes in three comparison Groups.(A, C, E). Bar plots illustrate the top enriched gene ontology (GO) terms categorized into biological process (blue), cellular component (green), and molecular function (orange) for CCM vs. ITR, CCM vs. WT , and WT vs ITR genes. The x-axis represents the GO term names, and the y-axis represents the number of genes associated with each GO term. (B, D, F). bubble plots of KEGG pathway enrichment analysis showing significantly enriched pathways for CCM vs. ITR, CCM vs. WT , and WT vs. ITR genes. The x-axis indicates the rich factor, and the y-axis lists the pathway names. The bubble size represents the number of genes enriched in each pathway, and the color gradient denotes the statistical significance (q-value) of enrichment, with red indicating more significant values and blue less significant.

cytoplasmic translation (GO:002181). In the cellular component category, cytoplasm (GO:0005737), plasma membrane (GO:0005886), nucleus (GO:0005634), and extracellular region (GO:0005576) were predominant. For molecular function, ATP binding (GO:0005524), metal ion binding (GO:0046872), and transmembrane transporter activity (GO:0022857) were the most enriched (Figure 6 (A,C,E)).

The KEGG pathway enrichment bubble plot revealed multiple pathways associated with pathogenic mechanisms across all three comparisons. In the CCM vs. ITR group, enrichment was observed in aminoacyl-tRNA biosynthesis (tve00970), styrene degradation (tve00643), fatty acid biosynthesis (tve00610), amino sugar and nucleotide sugar metabolism (tve00520), and ABC transporters (tve02010), suggesting roles in metabolism, biosynthesis, detoxification, and stress adaptation (Figure 6(B)). In CCM vs. WT group, the KEGG pathway analysis revealed DEGs enrichment in chemical carcinogenesis (tve05204), drug metabolism (tve00983), and longevity regulating pathway (tve04212) (Figure 6(D)). Tyrosine metabolism (tve00350), styrene degradation (tve00643), and amino sugar and nucleotide sugar metabolism (tve00520) were the most significant pathways in the WT vs. ITR group (Figure 6(F)).

To investigate the transcriptional responses of *T. verrucosum* under different groups, we conducted RNA-Seq analysis and visualized differentially expressed genes (DEGs) using hierarchical clustering heatmap. As shown in Figure 7(A), the gene expression patterns varied significantly among WT, ITR, and CCM groups. The CCM-treated samples exhibited widespread downregulation of genes (blue color), indicating a possible suppressive effect of classical Chinese herbal components on fungal gene activity. In contrast, the ITR-treated group showed extensive upregulation (red color) of numerous genes, suggesting a strong transcriptional activation in response to antifungal stress. The WT group demonstrated an intermediate expression profile, with partial overlap between CCM and ITR conditions. Hierarchical clustering of both genes and samples further confirmed that the three groups formed distinct expression clusters, highlighting the unique impact of each treatment on the transcriptomic landscape of *T. verrucosum*. These observations suggest that both CCM and ITR elicit highly condition-specific regulatory responses, potentially related to fungal growth inhibition and stress adaptation. To further explore the potential link between treatment and fungal virulence, we examined the expression of pathogenicity-related genes under wild-type and treated conditions. Several key virulence-associated genes were differentially expressed between WT and treated (TR) isolates as shown in Figure 7(B). Notably, gene-Tve07195 and gene-Tve04846 were significantly

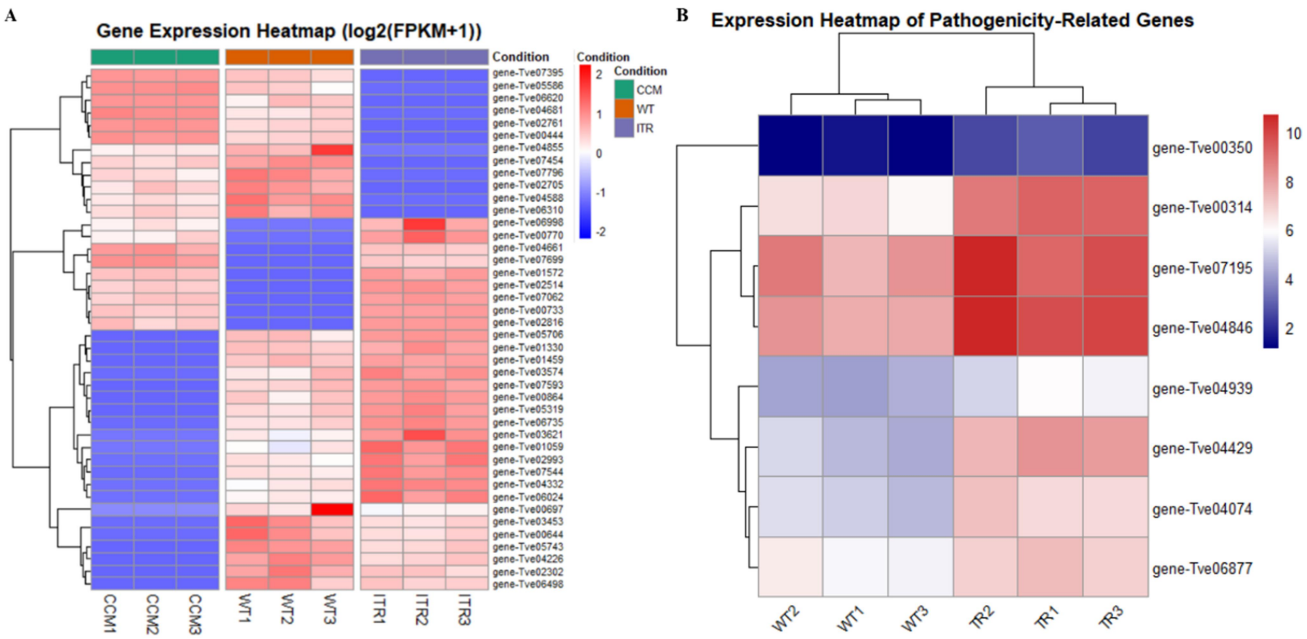

Figure 7. Transcriptomic profiling of differentially expressed and pathogenicity-related genes in *Trichophyton verrucosum*. (A). Heatmap of differential gene expression. This panel displays the expression patterns of differentially expressed genes (DEGs) across three experimental groups (WT, ITR, and CCM), based on $\log_2$(FPKM +1)) values. Each row represents a gene with differential expression, and each column corresponds to a biological replicate from each sample group. Red indicates the upregulated genes, while blue indicates downregulated genes. (B). Expression heatmap of pathogenicity-related genes. This heatmap shows the expression levels of selected pathogenicity-related genes in *T. verrucosum*, presented as log-transformed FPKM values. Red indicates high expression, while blue indicates low expression, providing insight into the transcriptional regulation of virulence-associated genes under different treatment conditions.

upregulated in treated samples (TR1–TR3) compared to all WT replicates. This upregulation may reflect an adaptive response mechanism that enhances pathogenic potential under itraconazole-induced stress. In contrast, gene-Tve00350 and gene-Tve04939 remained consistently lowly expressed across both conditions, suggesting limited or context-dependent roles in virulence regulation.

Integration of key functional modules in DEGs

To strengthen the interpretation of differential expression results, enriched GO terms and KEGG pathways were further organized into three major functional modules: virulence, antifungal response, and host adaptation. Virulence-associated functions were supported by enrichment in proteolysis (GO:0006508), cell wall organization, and amino acid transport, which are critical for host tissue degradation, nutrient acquisition, and fungal invasion. These findings are consistent with the observed modulation of proteolytic activity and structural components involved in pathogenicity.

Antifungal response mechanisms were strongly represented, particularly in the WT vs. ITR comparison, by enrichment in drug metabolism – cytochrome P450 (tve00982), ABC transporters (tve02010), and stress-related pathways including MAPK signaling, peroxisome, and autophagy. Additionally, significant enrichment of ribosome, aminoacyl-tRNA biosynthesis, and mRNA surveillance pathways indicates disruption of protein synthesis and activation of cellular stress responses under itraconazole treatment.

Host adaptation processes were reflected by enrichment in fatty acid biosynthesis (tve00610), amino sugar and nucleotide sugar metabolism (tve00520), and transmembrane transporter activity (GO:0022857), indicating metabolic reprogramming and membrane adaptation to environmental and antifungal stress. CCM treatment showed comparatively moderate enrichment in protein catabolism, oxidative stress response, and transport processes, suggesting a more targeted and less disruptive transcriptional response.

Overall, these results demonstrate that itraconazole induces extensive metabolic disruption, translational inhibition, and stress-response activation, whereas CCM promotes controlled metabolic adaptation and stress tolerance. These prioritized functional modules are summarized in the proposed model (Figure 8), providing a clearer mechanistic link between DEGs, pathogenicity, and antifungal response in *T. verrucosum*.

Transcriptomic analysis of transporter, detoxification, and infection-related genes under different treatments

To understand the molecular response of *T. verrucosum* to antifungal agents, we examined differentially expressed transporter, detoxification, and metabolism-related genes under CCM and ITR treatments in comparison to the control (wild type, WT) (Table 4). Several ABC (ATP-binding cassette) and MFS (Major Facilitator Superfamily) transporters, as well as cytochrome P450 enzymes, were differentially expressed in the CCM vs. WT group. ABC transporters, cytochrome P450s, MFS transporter, and ammonium transporter (Ato3) were upregulated while MFS multidrug transporters, vacuolar ATPase regulators, and amino acid/polyamine transporters were downregulated in CCM vs. WT group. In CCM vs. ITR, cytochrome P540 alkane hydrolase (gene-Tve04661) was up-regulated, whereas glutathione S-transferase, and multiple MFS transporters were down-regulated. MFS multidrug transporters, MFS glucose transporter, calcium ATPase, glucosamine-6-phosphate deaminase, and cytochrome P540 monooxygenase had the highest expression whilst ABC transporters, sterol biosynthesis enzymes, and MFS and other nutrient transporters had the lowest expression in WT vs. ITR group, revealing distinct expression under different comparison groups at the transcriptomics level.

Modulation of Subtilase, LysM, and transporter genes

Differential expression of genes encoding infection-related proteins in *Trichophyton verrucosum* was assessed under specific conditions using transcriptomic analysis (Table 5). Seven genes (gene-Tve00314, Tve00350, Tve04074, Tve04429, Tve04939, Tve06877, Tve07195) encode Subtilase with the PF00082 domain. Downregulation of these Subtilase genes (log2FoldChange from −1.14 to −3.25) suggests suppression of infection-related enzymatic activity under the tested conditions. This may reflect a host immune response, antifungal treatment, or altered environmental conditions inhibiting these virulent factors. Gene-Tve04429 showed the highest downregulation (−3.25), indicating a significant suppression of its expression, suggesting its important role in the pathogen's infection strategy.

Additionally, gene-Tve04846 contains the PF00188 (LysM domain), which indicates a reduced immune evasion capability under the tested condition. This

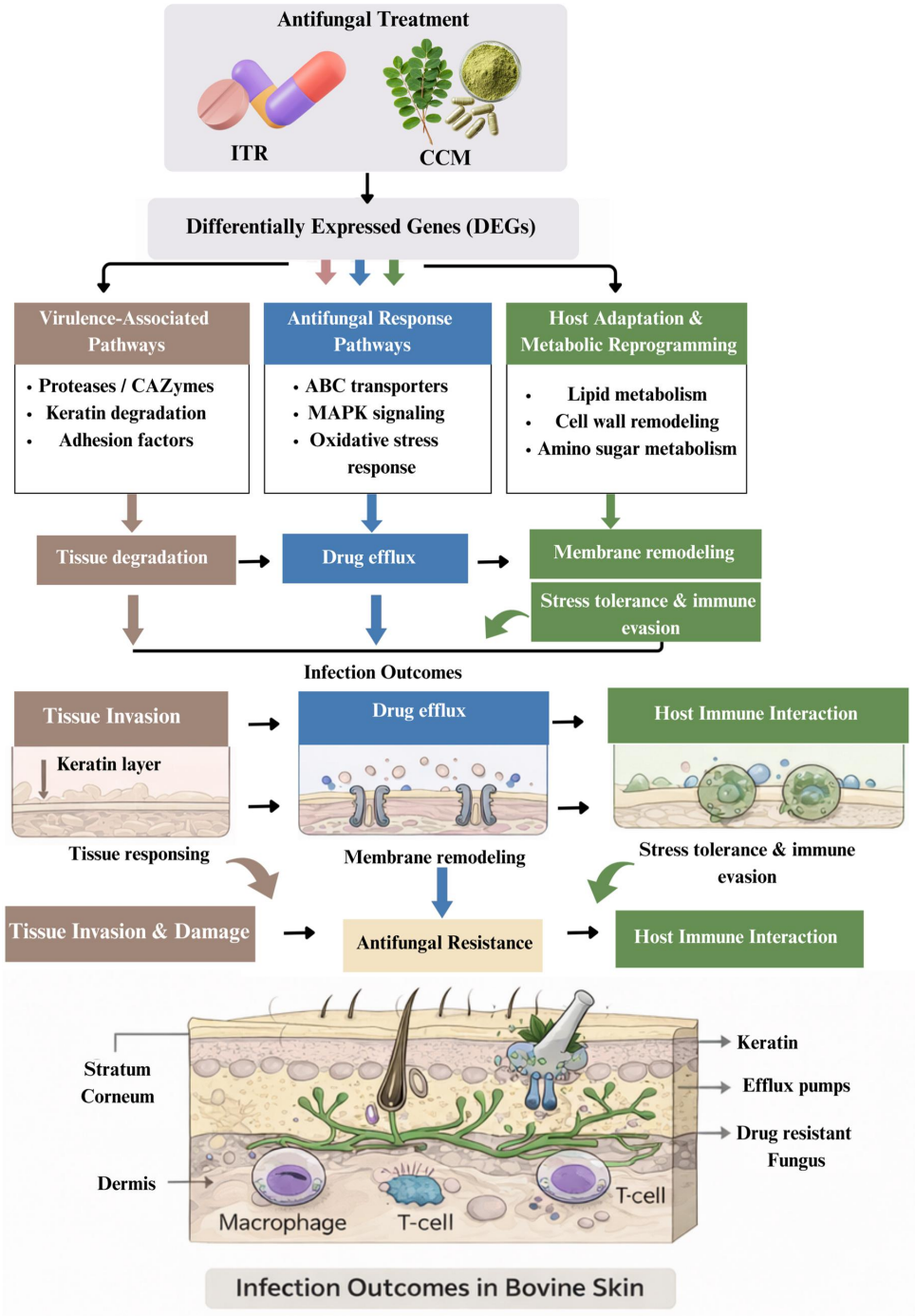

Figure 8. Model of differential expression results in virulence, antifungal response, and host adaptation in *Trichophyton verrucosum* under itraconazole and ccm treatments. This model summarizes the key functional modules identified in the differential expression results (DEGs) of *T. verrucosum*. The figure shows how DEGs in virulence-associated pathways (proteolysis, cell wall organization), antifungal response pathways (cytochrome P450s, ABC transporters), and host adaptation processes (fatty acid biosynthesis, amino sugar metabolism) contribute to tissue invasion, drug resistance, and immune evasion. The results show that itraconazole (ITR) induces extensive metabolic disruption, translational inhibition, and stress response activation, while ccm promotes controlled metabolic adaptation and stress tolerance.

Table 4. Key genes differentially expressed in wt, ITR, and ccm strains.

Samples	Gene ID	Description	log2FoldChange	Regulation
CCMVSWT	gene-Tve04681	ABC multidrug transporter	2.25	Up
CCMVSWT	gene-Tve07395	ABC multidrug transporter MDR3, Multidrug resistance protein 3	1.38	Up
CCMVSWT	gene-Tve05586	Cytochrome P450, putative	1.58	Up
CCMVSWT	gene-Tve06620	Cytochrome P450 monooxygenase, putative	1.08	Up
CCMVSWT	gene-Tve04588	MFS multidrug transporter	−1.11	Down
CCMVSWT	gene-Tve04855	Putative MFS multidrug transporter	−3.21	Down
CCMVSWT	gene-Tve07796	Putative MFS sugar transporter Stl1	−1.34	Down
CCMVSWT	gene-Tve02761	MFS multidrug transporter, putative	1.54	Up
CCMVSWT	gene-Tve04588	MFS multidrug transporter	−1.11	Down
CCMVSWT	gene-Tve04855	Putative MFS multidrug transporter	−3.21	Down
CCMVSWT	gene-Tve00444	Plasma membrane ammonium transporter (Ato3), putative	1.35	Up
CCMVSWT	gene-Tve02705	Amino acid/polyamine transporter I	−2.42	Down
CCMVSWT	gene-Tve06310	Regulator of V-ATPase in vacuolar membrane protein	−1.31	Down
CCMVSWT	gene-Tve07454	Protein required for cell viability Rrp17, putative	−1.31	Down
CCMVSITR	gene-Tve00733	Glutathione S-transferase, putative	−2.60	Down
CCMVSITR	gene-Tve02816	MFS peptide transporter	−1.68	Down
CCMVSITR	gene-Tve02514	Putative MFS sugar transporter	−1.11	Down
CCMVSITR	gene-Tve06998	MFS transporter, putative	−1.76	Down
CCMVSITR	gene-Tve07062	Putative MFS transporter	−1.08	Down
CCMVSITR	gene-Tve04661	Cytochrome P450 alkane hydroxylase	1.06	Up
CCMVSITR	gene-Tve00770	Cytochrome P450, putative	−1.61	Down
CCMVSITR	gene-Tve01572	Cytochrome P450, putative	−1.05	Down
CCMVSITR	gene-Tve07699	ABC multidrug transporter, putative	1.12	Up
WTVSITR	gene-Tve01330	ABC multidrug transporter	−1.42	Down
WTVSITR	gene-Tve02993	ABC multidrug transporter, putative	−1.45	Down
WTVSITR	gene-Tve01459	C-8 sterol isomerase (Erg-1), putative	−1.21	Down
WTVSITR	gene-Tve04332	Sterol 24-C-methyltransferase, EC:2.1.1. Delta (24)-sterol C-methyltransferase	−3.15	Down
WTVSITR	gene-Tve05743	Cytochrome P450 monooxygenase, putative	1.04	Up
WTVSITR	gene-Tve03574	Cytochrome P450 alkane hydroxylase, putative	−2.07	Down
WTVSITR	gene-Tve05319	MFS transporter, putative	−1.35	Down
WTVSITR	gene-Tve05706	MFS monosaccharide transporter, putative	−1.30	Down
WTVSITR	gene-Tve06024	MFS monocarboxylate transporter, putative	−1.05	Down
WTVSITR	gene-Tve03453	MFS multidrug transporter, putative	2.55	Up
WTVSITR	gene-Tve03621	MFS transporter	−1.74	Down
WTVSITR	gene-Tve00864	Putative MFS transporter	−1.52	Down
WTVSITR	gene-Tve00697	MFS multidrug transporter, putative	4.72	Up
WTVSITR	gene-Tve00644	MFS glucose transporter, putative	2.55	Up
WTVSITR	gene-Tve02302	MFS multidrug transporter, putative	1.10	Up
WTVSITR	gene-Tve01059	Transporter	−2.42	Down
WTVSITR	gene-Tve06498	Calcium transporting ATPase (Pmc1), putative	1.52	Up
WTVSITR	gene-Tve06735	Protein transport membrane glycoprotein Sec20, putative	−1.43	Down
WTVSITR	gene-Tve07593	Amino acid transporter, putative	−1.46	Down
WTVSITR	gene-Tve07544	Choline transporter Hnm1, putative	−1.95	Down
WTVSITR	gene-Tve04226	Glucosamine-6-phosphate deaminase	1.48	Up
WTVSITR	gene-Tve00733	Glutathione S-transferase, putative	−2.60	Down
WTVSITR	gene-Tve04226	Glucosamine-6-phosphate deaminase	3.11	Up

may reflect ineffective colonization or an adaptive trade-off during treatment.

Further analysis revealed modulation of transporter genes, which are critical for fungal pathogenicity, stress response, and antifungal resistance. Genes such as MFS multidrug transporters (e.g. Tve03453, Tve00697), ABC multidrug transporters (e.g. Tve04681), and Plasma membrane ammonium transporter (e.g. Tve00444) were upregulated, indicating their potential involvement in drug resistance and nutrient acquisition under stress. Conversely, gene-Tve01059 (another transporter) was downregulated, suggesting an alteration in transport capacity under the tested conditions. Additionally, cytochrome P450 (e.g. Tve05586) was upregulated, indicating its role in metabolic adaptations and stress response mechanisms.

These findings, including the modulation of Subtilase, LysM, and transporter genes, further confirm the robustness of our transcriptomic analysis and highlight the complex regulatory networks involved in fungal adaptation and virulence.

Validation of RNA- Seq by qRT- PCR

qRT-PCR of selected DEGs confirmed the RNA-Seq expression patterns in the WT vs. ITR (Figure 9(A)), and WT vs. CCM comparisons (Figure 9(B)). The qRT-PCR results were consistent with the RNA-Seq data, confirming the reliability of the transcriptomic analysis. Pearson's correlation revealed a strong positive correlation between qRT-PCR and RNA-Seq expression levels ($r = 0.67$, $p < 0.001$), indicating a high degree of consistency between the two methods.

Table 5. Differential expression of genes involved in virulence and transporter pathways in *Trichophyton verrucosum*.

Gene ID	Protein Domain	Functional Description	Log2 Fold Change	Regulation
gene-Tve00314	PF00082	Subtilisin-like serine protease involved in host protein degradation and nutrient acquisition during infection.	−2.60	Down
gene-Tve00350	PF00082	Secreted serine endopeptidase facilitating tissue penetration and keratin degradation in host skin.	−1.83	Down
gene-Tve04074	PF00082	Extracellular subtilase linked to virulence, involved in hydrolyzing structural host proteins like keratin.	−1.98	Down
gene-Tve04429	PF00082	Virulence-associated protease contributing to host invasion and fungal colonization via proteolytic activity.	−3.25	Down
gene-Tve04939	PF00082	Serine protease associated with extracellular digestion and host-pathogen interaction mechanisms.	−1.34	Down
gene-Tve06877	PF00082	Subtilase enzyme implicated in protein turnover and fungal adaptability during host infection.	−1.14	Down
gene-Tve07195	PF00082	Proteolytic virulence factors involved in tissue invasion and stress-induced fungal response.	−1.74	Down
gene-Tve04846	PF00188	LysM domain-containing effector protein involved in immune evasion during fungal infection.	−2.26	Down
gene-Tve00697	MFS	Multidrug transporters involved in the efflux of antifungal compounds and metabolic regulation.	4.72	Up
gene-Tve04226	Glucosamine-6-phosphate deaminase	Enzyme involved in glucosamine metabolism and cell wall synthesis.	3.11	Up
gene-Tve04681	ABC	Multidrug ABC transporter associated with antifungal resistance.	2.25	Up
gene-Tve05586	Cytochrome P450	Cytochrome P450 | Enzyme involved in the metabolism of xenobiotics and stress response.	1.58	Up
gene-Tve00444	Ammonium transporter	Ammonium transporter | Plasma membrane transporter involved in ammonium uptake and pH regulation.	1.35	Up
gene-Tve03453	MFS	Multidrug transporter involved in resistance to antifungal agents.	2.55	Up
gene-Tve01059	Transporter	Membrane transporter implicated in nutrient uptake.	−2.42	Down
gene-Tve04855	MFS	Multidrug transporter involved in nutrient and drug efflux.	−3.21	Down

Discussion

A high-quality genome of Trichophyton verrucosum was assembled

Dermatophyte infections are a serious global health concern affecting both humans and animals, with the potential to spread zoonotically and cause outbreaks among exposed populations [95,96]. *Trichophyton verrucosum*, a dermatophyte species commonly isolated from skin lesions of beef cattle, also affects other domestic animals and humans, causing cattle ringworm-a condition prevalent in many countries [95]. In China, the Xinjiang Uygur Autonomous Region reports a high incidence of *T. verrucosum* infections in both cattle and humans [97]. This study integrated whole-genome sequencing (PacBio, Illumina, and Hi-C platforms) with transcriptome (RNA-Seq) analysis to construct a comprehensive genome map and identify genes differentially expressed under antifungal treatment. The assembled genome of *T. verrucosum* is 23.44 Mb in size and encodes 7,936 protein-coding genes, with 98.8% completeness assessed by BUSCO. The transcriptional profiling provided functional insights into gene expression dynamics, especially those related to keratin degradation, oxidative stress response, transporters, and secondary metabolism. Collectively, the genome and transcriptome data provide a strong foundation for investigating the molecular mechanisms underlying *T. verrucosum* pathogenicity, host adaptation, and potential drug resistance.

Genome sequencing has become a fundamental approach for investigating the biology and ecological potential of fungi, offering unparalleled insights into their genetic composition, metabolic pathways, and adaptive strategies [98,99]. Whole-genome sequencing (WGS) is anticipated to transform the infectious disease surveillance and diagnosis owing to its great resolution [100]. Among advanced sequencing technologies, Pacific Biosciences' single-molecule real-time (SMRT) sequencing offers long reads of up to 23,000 bp and a yield of ~1,080 Mb per run, providing high-quality data well-suited for assembling complex genomes. However, the PacBio RS platform produces raw reads with relatively high error rates, reported to reach up to 17.9% [101]. While widely applied for viruses, bacteria, and small-genome organisms, its use in pathogenic fungi has been limited. This is largely due to common challenges in fungal genome assembly, including enormous genomic sizes, increased heterozygosity, and intricate repetitive regions [102]. These complications

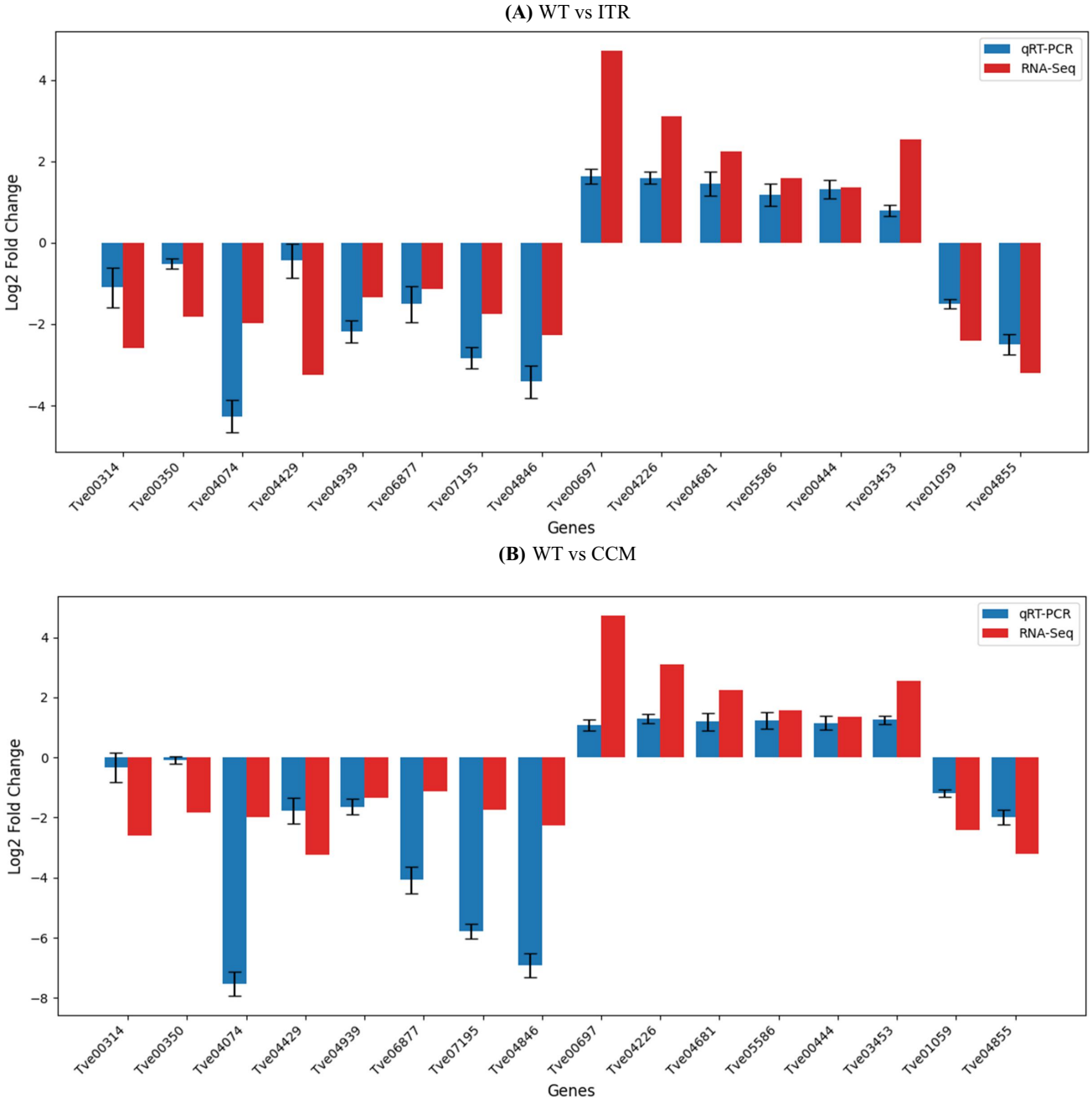

Figure 9. Comparison of qRT- PCR and RNA- Seq expression ratios for selected genes. (A).Bar chart depicting the gene expression profiles of 16 selected genes as measured by qRT-PCR (blue bars) and RNA-Seq (red bars) comparing wild-type (WT) vs. itraconazole-treated (ITR) samples. The x-axis represents the gene and the y-axis represents the $\log_2$ Fold change in expression levels. Error bars indicate the standard error of qRT-PCR measurements. This figure highlights the consistency and differences between the two methods across genes in response to ITR treatment. (b). Bar chart depicting the gene expression profiles of the same 16 selected genes as measured by qRT-PCR (blue bars) and RNA-Seq (red bars) comparing wild-type (WT) vs. CCM-treated samples. Log_2 Fold changes are presented on the y-axis, with qRT-PCR error bars representing standard errors. The figure allows comparison of transcriptional responses measured by both techniques under ccm treatment, illustrating variations in expression modulation between treatments.

can hinder genome assembly and annotation, making it difficult to obtain a complete and accurate fungal genome [103]. We generated a high-quality, chromosome-level genome assembly of *T. verrucosum* (GenBank: OR056436.1) using PacBio, Illumina, and Hi-C sequencing. The assembly spans 23.44 Mb, includes 7,936 predicted protein-coding genes, and has an average coverage of 230.9 X. These metrics are comparable to prior reports: for example [33], described a *T. verrucosum* genome of 24.17 Mb, with a GC

content of 48.24%, a repeat content of 2.13%, and 8,024 predicted protein-coding genes. Similarly, the genome of *Arthroderma benhamiae* was 22.3 Mb with 7,980 predicted genes, 5,809 genes with introns, and 80 tRNA genes [32]. Another related species, *Trichophyton schoenleinii* possesses a genome of 23.67 Mb, with three chromosomes, a GC content of 47.31%, and 7,474 predicted genes [104]. These comparisons underscore the high quality and reliability of our *T. verrucosum* genome assembly and provide a foundation for deeper comparative and functional genomics analysis.

Draft genomes of dermatophytes show strong conservation at both nucleotide and amino acid levels, reflecting evolutionary constraints and shared pathogenic mechanisms among these fungi [33]. In our study, the genome of *T. verrucosum* demonstrated a high level of completeness, with 98.8% of BUSCO detected (Table 1). This proportion surpasses that of several closely related keratinophilic fungi, including *Arthroderma uncinatum* (97.3%) [105], *Chrysosporium keratinophilum* (96%) [106], and *Malbranchea zuffiana* (95.7%) [107], while slightly lower than *T. mentagrophytes* (99.1%) and *T. tonsurans* (99%) [108]. This high BUSCO completeness reflects the superior quality and integrity of *T. verrucosum* genome assembly, establishing it as a valuable reference for dermatophyte comparative genomics.

In the *T. verrucosum* genome, transposable elements (TEs) comprise approximately 3.64% of the total sequence (Table 2). The structural organization and distribution of repetitive regions within the fungal genome facilitate the identification of the optimal approach for whole-genome sequencing [109]. With the increasing availability of high-quality fungal genome assemblies, recent advances have enabled large-scale comparative studies across the fungal kingdom, including detailed TE landscape analyses [110,111]. Studies indicate that animal-associated and pathogenic fungi possess higher TE content than other fungi, potentially contributing to effector gene diversification [112,113]. Our study found that TEs had the maximum percentage of DNA transposons (2.37%), followed by LTR (0.73%) and LINE (0.53%). Although the overall TE content in *T. verrucosum* is lower than in *Neurospora crassa* (10%), or *S. cerevisiae* (6%) [110,114], and higher than in *Fusarium graminearum* (0.1%), and *Trichoderma species* (0.48%) [115,116]. Even among related species, such as genus *Paracoccidioides* there are differences in their TE concentrations. TEs make up 8–9% of the genome in *Paracoccidioides brasiliensis* and twice as much (16%) in *Paracoccidioides lutzii* [117]. Furthermore, comparison with closely related dermatophytes reveals that TE content varies across species, including 1.73% in *T. rubrum*, 3.70% in *T. tonsurans*, 7.20% in *T. equinum*, 2.43% in *M. canis*, 1.54% in *M. gypseum*, and 1.34% in *A. benhamiae* [32]. The TE proportion in *T. verrucosum* (3.64%) falls within this range, indicating a conserved repeat landscape and limited TE expansion among dermatophytes.

T. verrucosum revealed 262 distinct metabolic pathways, providing insights into metabolic capacity and its potential for adaptation to host-associated environments. A substantial proportion of annotated genes were associated with key metabolic processes, including carbohydrate metabolism, amino acid biosynthesis, lipid metabolism, and energy metabolism, underscoring the fungus's capacity to adapt and survive in the nutrient-limited conditions of keratinized host tissues. During host colonization, glycolysis/gluconeogenesis, oxidative phosphorylation, and the tricarboxylic acid (TCA) cycle were identified as prominent energy-generating pathways [33]. In addition to primary metabolism, genes involved in xenobiotic degradation and secondary metabolite biosynthesis were also annotated. KOG classification further identified 4,861 genes grouped into categories related to cellular processes and signaling, metabolism, and information storage and processing, highlighting the intricate regulatory networks governing fungal growth, host adaptability, and stress response. Notably, the predominance of signal transduction and transcriptional regulation genes implies extensive environmental sensing systems, likely facilitating invasion of bovine skin, hooves, and hair. Comparable gene expansions were reported in *A. benhamiae* and *Trichophyton interdigitale*, where they contribute to host-specific pathogenic traits [10,11]. AntiSMASH analysis identified putative secondary metabolite biosynthetic gene clusters, including NRPS, PKS, and hybrid NRPS – PKS clusters, which are often associated with virulence, microbial competition, and immune evasion [118]. Our analysis identified diverse secondary metabolite biosynthetic gene clusters across seven fungal genomes, with *T. verrucosum* containing 34 clusters, including 12 NRPS and 7 PKS genes. Compared with other dermatophytes, *M. gypseum*, *M. canis*, *A. benhamiae*, *T. rubrum*, and *T. tonsurans*, which harbor fewer or no NRPS and nonreducing PKS genes, *M. gypseum* possesses more PKS genes (6), and *M. canis* carries additional nonreducing and reducing PKS genes, likely contributing to enhanced host colonization [33]. The broad diversity of secondary metabolism gene clusters in *Arthrodermataceae* species highlights significant

variation among closely related fungi and suggests that this diversity plays a key role in epidermal colonization [32].

The richness and diversity of pathogenic factors in Trichophyton verrucosum

We studied the pathogenic mechanism of *Trichophyton verrucosum* using several databases, including those for carbohydrate-active enzymes (CAZymes), pathogen–host interaction genes (PHIs), and database of fungal virulence factors (DFVF). CAZymes, comprising a wide range of carbohydrate-active and accessory enzymes, enable fungi to degrade and modify complex biomass, supporting their survival in diverse environments. Numerous CAZymes are secreted through specialized enzyme secretion systems, which are highly developed in filamentous fungi [119]. CAZymes play crucial roles in the survival and pathogenesis of fungi by breaking down the host's components, allowing the fungus to uptake nutrients and develop a successful infection process [120]. CAZymes function by degrading, synthesizing or modifying glycosidic linkages in glycoconjugates and oligo- and polysaccharides, with essential roles in cell wall construction, signaling, and energy generation [121].

CAZyme analysis of the *T. verrucosum* genome identified 1,157 genes across diverse Came families, with glycoside hydrolases (GHs) being the most abundant, accounting for 562 genes (48%). These enzymes catalyze the cleavage of glycosidic bonds, either between carbohydrates or between a carbohydrate and a non-carbohydrate group [122]. In fungi, these enzymes pertain to feeding, growth, mycoparasitism, and pathogenicity [123]. Glycosyltransferases (GTs), the second most abundant family with 326 genes (28%), catalyze glycosidic bond formation by transferring sugar moieties from activated donors to specific acceptors [124]. A rising body of data indicates that by catalyzing glycosylation, glycosyltransferases are essential for hyphal development, conidiation, stress responses, and host–pathogen interactions [125]. Other identified CAZymes families include auxiliary activity (AAs) with 116 genes (10%), carbohydrate-binding module (CBMs) with 100 genes (9%), carbohydrate esterases (CEs) with 44 genes (4%), and polysaccharide lyases (PLs) with 9 genes (1%) (Figure 3(A)).

PHI-base is a curated database of experimentally validated virulence-related genes influencing pathogen – host interactions [126]. PHI analysis of the *T. verrucosum* genome identified 2,920 putative PHI genes (Figure 3(B)). Of these, 1,427 genes were linked to reduced virulence, 918 to unaltered pathogenicity, and 248 to loss of pathogenicity, suggesting that *T. verrucosum* may exhibit moderate pathogenicity due to the prevalence of reduced and unaltered virulence genes. Additionally, 166 genes were associated with increased virulence, 113 with lethal phenotypes, and 17 with chemical resistance.

Protease secretion is another crucial factor in *T. verrucosum* pathogenicity, particularly in keratin degradation. Previous genomic studies have confirmed an enrichment of protease genes in dermatophytes [33,127]. Among the secreted proteases, extracellular endoproteases such as subtilisin (S8A family), and fungalysin (M36) are common in dermatophytes [128]. DFVF database analysis identified 15 distinct virulence factors with varying gene counts and functional roles (Figure 3(C)). For instance, *T. rubrum* contains five endo metalloprotease (MEP) genes and seven serine protease (SUB) genes [129]. Similarly, genes such as SUB1–3 and MEP1–3 have been identified in *M. canis*; SUB1–7 in *E. floccosum*; SUB3 and SUB6 in *T. benhamiae*; and multiple SUB genes in *T. verrucosum* and *M. gypseum* [130–134]. Our analysis found that *T. verrucosum* contains 12 copies of SUB1 gene, which may contribute to its ability to infect keratinized tissues including nails. In *T. rubrum*, SUB7 is most highly expressed gene during nail infection which is the most common dermatophyte in China [135]. PCR- based screening confirmed the presence of multiple subtilisin (Sub1-7) and fungalysin (Mep1-5) genes, which are essential for host invasion and nutrient acquisition. Expression analysis of *A. benhamiae* during growth on keratin and cutaneous infection of guinea pigs revealed the upregulation of fungalysin and subtilisin genes using cDNA microarray analysis [136]. Although many dermatophytes carry SUB1 and SUB3-7, but their enzyme panels are incomplete: SUB4-7 genes are absent in *M. canis* [129]. Nevertheless, SUB1 and SUB3 have been shown to enhance virulence and adherence to keratinized stratum corneum in *M. canis* [137–139]. The consistent amplification of SUB1 and SUB2 across *T. verrucosum* suggests that SUB1 may serve as an evolutionary marker and key contributor to keratin degradation and infection.

Comparative genomics of Trichophyton verrucosum

Our comparative genomic analysis revealed that *Trichophyton verrucosum* exhibited the close genetic relationship with *T. rubrum*, showing significant chromosomal similarities, followed by *M. gypseum* and *M. canis*. Although genomic data on *T. verrucosum* remain limited, studies on *T. rubrum* [33], *T.*

schoenleinii [104], and *E. floccosum* [140] are valuable for understanding evolutionary patterns. The genome of *T. rubrum* has been sequenced and compared with other dermatophyte species to identify potential genes implicated in infections of human skin and nail infections. Additionally, the genomes of other related species, such as *T. tonsurans*, *T. equinum*, *M. canis*, and *M. gypseum*, exhibit evolutionary gene duplications and are enriched in genes encoding proteases, kinases, secondary metabolites, and lysine motif (LysM) effectors, which may enhance their pathogenic potential [33]. While these six species were differed from *T. verrucosum* in genomic architecture and phenotypic traits, all seven pathogens share 393 core orthogroups. Further investigation is required to determine how these core genes contribute to the pathogenesis of bovine dermatophytosis.

We identified 393 genes in species-specific orthogroups, including 184 single-copy orthogroups conserved across all analyzed species. These core genes are likely essential for fungal survival and key cellular functions, including nutrient acquisition, keratin degradation, and stress adaptation, aligning with findings from previous pan-genome studies in dermatophytes [32,33], which suggests that these core genes encode fundamental cellular processes for survival on keratinized tissues. Notably, *T. verrucosum* showed a complete absence of species-specific orthologs, indicating a highly conserved genomic structure. This contrasts with other dermatophytes like *T. tonsurans* and *T. rubrum*, which possess 805 and 9,267 distinct genes, respectively. These results align with the findings of [33], who reported that *T. verrucosum* exhibits a high amino acid similarity with *T. rubrum*, implying tight evolutionary ties and strong genetic conservation. The absence of novel genes in *T. verrucosum* supports the concept that its virulence and host specificity are primarily influenced by gene control and the functional optimization of conserved gene sets than by the emergence of new genes. This is further supported by [10], who emphasized the need for enhanced phylogenetic revolution within dermatophytes, primarily in relation to their genomic stability. However, our findings support the hypothesis that dermatophyte evolution, especially in zoophilic species such as *T. verrucosum* is predominantly influenced by gene regulation, adaptation of conserved proteins, and ecological pressures, rather than by horizontal gene transfer or de novo gene emergence [10,33,128].

The 393 core orthogroups, including 184 single-copy genes, represent a conserved genomic backbone across dermatophytes and are primarily associated with essential functions such as metabolism, cellular maintenance, and core pathogenic processes (e.g. keratin utilization and stress response). Their conservation across species supports a shared molecular framework for survival and colonization of keratinized tissues. In contrast, divergence in non-core gene content likely underlies differences in host range and pathogenicity, with lineage-specific adaptations contributing to variation in host preference and infection strategies (Figure 4).

Transcriptome profiling of Trichophyton verrucosum

RNA-seq is a powerful tool in molecular genetics that enables comprehensive analysis of gene expression patterns, facilitating a more profound understanding of complex biological processes. The current study provides a comprehensive transcriptomic analysis of *T. verrucosum* by examining gene expression patterns between control and treatment groups. A total of 1,880 genes were differentially expressed, with 936 significantly upregulated and 944 downregulated. Notably, 21 genes were consistently regulated across all comparisons, indicating conserved fungal stress response mechanisms. GO and KEGG enrichment analyses showed that ITR and CCM treatments significantly altered key biological processes and molecular functions. GO terms were enriched for proteolysis, amino acid transport, cytoplasmic translation, ATP binding, and transporter activity. KEGG pathways with notable changes included amino sugar and nucleotide sugar metabolism, fatty acid biosynthesis, drug metabolism, tyrosine metabolism, and ABC transporters (Figure 5, 6).

Transcriptome profiling of *T. verrucosum* also uncovered differentially expressed genes involved in transport, detoxification, and metabolism in response to ITR and CCM treatments. Multidrug resistance, which is defined by the development of structural and chemical resistance to several drugs, presents a significant challenge in the treatment of fungal infections. Multidrug resistance in fungi is caused by several metabolic processes. The most prevalent mechanisms are increased drug efflux, modifications at the drug target region, and decreased drug absorption [141]. The last mechanism is mostly mediated by transmembrane transporters that are members of the major facilitator superfamily and the ATP-binding cassette superfamily (ABC) [142]. Several transmembrane transporter genes from the ABC and MFS families were upregulated, including Tve04681 ($\log_2$ Foldchange: 2.25), Tve02761 (1.54), Tve07699 (1.12), Tve03453 (2.55), Tve00697 (4.72), and Tve02302 (1.10) (Table 4). The primary mechanism of resistance

in dermatophyte species seems to be drug efflux [143]. In fact Fachin et al. [144] found that terbinafine increased the expression of the TruMDR2 ABC-transporter gene in *T. rubrum*. Additionally, the ΔTruMDR2 mutant strain exhibited diminished infectivity and reduced growth on human nails compared to the wild-type strain [145]. Collectively, our results suggest that ABC and MFS may contribute to the resistance and pathogenicity of *T. verrucosum*.

Cytochrome P450 monooxygenases (CYP450s), a diverse group of heme-thiolate enzymes, play essential roles in primary and secondary metabolism [146]. These enzymes play a crucial role in steroid conversion and heterogeneous metabolism, as well as in the catalysis of oxidative reactions involving a variety of organic substrates [147]. Transcriptomic analysis revealed differential expression of multiple CYP genes in *T. verrucosum*, suggesting roles in stress response and potential drug resistance. Notably, Tve05586 and Tve06620, encoding putative cytochrome P450 monooxygenases, were significantly upregulated in CCM vs. WT. Similarly, in the CCM vs. ITR comparison, a mixed expression pattern was observed with gene-Tve04661 (log_2 Fold Change: 1.06), annotated as cytochrome P450 alkane hydroxylase which was upregulated, whereas gene-Tve00770, and gene-Tve01572 were downregulated. In WT vs. ITR, gene-Tve03574 was strongly downregulated (log_2 Fold Change: −2.07), while gene-Tve05743 was slightly upregulated. Similar trends were previously observed in *Fusarium graminearum*, where Tebuconazole treatment increased the expression of two genes that encode the CYP450 monooxygenase, FGSG_03498 and FGSG_09195, by over 25- and 149-fold, respectively [148]. These findings support the role of fungal CYP450 enzymes in detoxifying fungicides and their metabolites [144,149,150]. Ergosterol is a crucial component of fungal cell membrane integrity and a primary target of azole antifungals, which inhibit the enzyme 14α-demethylase [151]. In our analysis, we found the repression of the ERG1 (gene-Tve01459, Log_2 Fold Change: −1.21) (Table 4). Likewise, itraconazole treatment repressed genes involved in ergosterol biosynthesis, including sterol 24-C-methyltransferase, EC:2.1.1. Delta (24)-sterol C-methyltransferase (gene-Tve04332, Log_2 Fold Change: −3.15). Notably, a previous cDNA microarray analysis of *T. rubrum* in response to terbinafine did not detect modulation of ERG1, suggesting species- or drug-specific regulation [152]. This study showed that *T. verrucosum* genes encoding known fungal virulence factors were modulated by ITR and CCM treatment. Secreted enzymes, which aid host tissue degradation and facilitate fungal invasion, emerged as key virulence factors [33]. During infection, each dermatophyte species is thought to regulate protease and virulence factor expression through host-specific regulatory systems [137]. For effective hyphal growth, dermatophytes secrete proteases and peptidases to degrade host proteins. Our transcriptomic analysis revealed that ITR and CCM treatments led to the downregulation of key virulence-related genes in *T. verrucosum*, including Subtilase (PF00082) and LysM domain-containing proteins (PF00188), which are involved in host protein degradation and immune evasion, respectively. These findings suggest that antifungal treatments disrupt the pathogen's infection mechanisms. Additionally, upregulation of MFS and ABC multidrug transporters, as well as cytochrome P450 enzymes, indicates the fungus's adaptive response to stress and potential involvement in drug resistance. These results confirm that treatment with ITR and CCM affects fungal virulence and resistance pathways (Figure 9).

This study highlights the value of integrating genomic and transcriptomic analyses to elucidate *T. verrucosum* pathogenicity. By identifying key virulence-associated genes and their regulatory networks, it provides a foundation for developing targeted antifungal therapies and advancing research on dermatophyte virulence mechanisms. These findings also support combining traditional antifungal treatments with genomic-based strategies, offering a path toward improved control of bovine dermatophytosis and other dermatophyte infections.

Conclusion

This study presents a high-quality, chromosome-level genome and transcriptome analysis of *T. verrucosum*, offering key insights into its pathogenic mechanisms and antifungal responses. The assembly identified 7,936 protein-coding genes, including those associated with virulence and drug resistance. Comparative genomics revealed a close evolutionary relationship with other dermatophytes, particularly *T. rubrum*, highlighting genomic features linked to pathogenicity. Transcriptomic profiling showed differential expression of genes involved in metabolism, stress response, and keratin degradation, with notable protease gene downregulation under antifungal treatments. These findings provide valuable targets for improved diagnostics and therapies, supporting better control of bovine dermatophytosis and related zoonotic infections.

Limitations in phenotypic species identification

The colony and microscopic morphology observed in this study align with the known variability reported for *T. verrucosum*. Hong et al. [153] described a cattle-derived isolate with slow-growing, folded, heaped, glabrous, and white colonies, along with chains of chlamydoconidia, consistent with our observations. Kane [154] also noted considerable variability in macroconidia and microconidia production, with chlamydospores being a more consistent feature. This variability supports chlamydospore formation and slow-growing colony morphology as reliable diagnostic traits. In this study, the isolate was cultured on SDAM, a nutrient-rich medium that may have influenced colony morphology, pigmentation, and sporulation patterns. The observed mild cream-to-pale yellow pigmentation and limited conidial production are biologically plausible, and the species identity was confirmed through ITS sequencing, phylogenetic analysis, ANI, and Mash distance analysis, ensuring accuracy despite the observed morphological variation. Regarding the urease test, while *T. verrucosum* is commonly reported as urease negative, the isolate in our study tested positive, showing a color change from yellow to pink after 3–5 days of incubation. This finding aligns with [155], who reported that urease activity can be observed in some *T. verrucosum* strains under certain conditions, despite the species typically being described as urease negative. Kim [156] further highlighted variability in urease activity across *T. verrucosum* isolates, reinforcing that urease activity should not be used as the sole criterion for species identification. We relied on molecular methods, including ITS sequencing and chromosome-level genome assembly, for definitive species identification. This approach is consistent with findings by Spanamberg et al. [157] and Łagowski et al. [158], which emphasize the reliability of PCR-based identification for bovine dermatophytes. While biochemical tests like the urease test are informative, molecular methods remain the most reliable for confirming *T. verrucosum* due to the morphological and biochemical variability observed across isolates.

Future recommendations and limitations

This study provides a solid genomic and transcriptomic foundation for *T. verrucosum*, but there are areas for improvement. Future research could benefit from long-read sequencing to enhance assembly quality and resolve repetitive regions. Expanding transcriptomic profiling with different antifungal treatments, time-course studies, and dose–response analyses is crucial. Functional validation of key genes related to virulence, stress adaptation, and antifungal resistance is needed, along with the use of CRISPR or reverse genetics. Including more dermatophyte species and host-specific strains in comparative genomics, and integrating proteomics and metabolomics, will help refine metabolic and regulatory networks. These efforts will improve diagnostics and enable the development of targeted antifungal therapies for bovine dermatophytosis and other zoonotic infections.

Acknowledgements

Muhammad Salman Tahir (MST): Conceptualization, Data curation, Methodology, Writing–original draft, Software, Visualization. Xiaoping Ma (XM): Conceptualization, Resources, Supervision, Visualization, Methodology, Funding acquisition, Writing – review & editing. Yu Gu (YG): Conceptualization, Resources, Methodology, Project Administration, Writing – review & editing, Visualization. Ruiguo Liu (RL), Yingchong Liao (YL), Xiangwen Zeng (XZ), Xing Zhao (XZ), Rongyan Luo (RL), Bingying Li (BL), Jianing Liu (JL), Haiye Yang (HY): Data curation, Formal analysis, Software, Visualization. Keying He (KH), Sha Ye (SY), Yan Tang (YT), Hongrui Guo (HG), Gang Ye (GY), Zhicai Zuo (ZZ): Formal analysis, Investigation, Visualization, Writing – review & editing. All authors read and approved the final manuscript.

Author contributions

CRediT: **Muhammad Salman Tahir:** Conceptualization, Data curation, Methodology, Software, Visualization, Writing – original draft; **Xiaoping Ma:** Conceptualization, Funding acquisition, Methodology, Resources, Supervision, Visualization, Writing – review & editing; **Yu Gu:** Conceptualization, Methodology, Project administration, Resources, Visualization, Writing – review & editing; **Ruiguo Liu:** Data curation, Formal analysis, Software, Visualization; **Yingchong Liao:** Data curation, Formal analysis, Software, Visualization; **Xiangwen Zeng:** Data curation, Formal analysis, Software, Visualization; **Xing Zhao:** Data curation, Formal analysis, Software, Visualization; **Rongyan Luo:** Data curation, Formal analysis, Software, Visualization; **Bingying Li:** Data curation, Formal analysis, Software, Visualization; **Jianing Liu:** Data curation, Formal analysis, Software, Visualization; **Haiye Yang:** Data curation, Formal analysis, Software, Visualization; **Keying He:** Formal analysis, Investigation, Visualization, Writing – review & editing; **Sha Ye:** Formal analysis, Investigation, Visualization, Writing – review & editing; **Yan Tang:** Formal analysis, Investigation, Visualization, Writing – review & editing; **Hongrui Guo:** Formal analysis, Investigation, Visualization, Writing – review & editing; **Gang Ye:** Formal analysis, Investigation, Visualization, Writing – review & editing; **Zhicai Zuo:** Formal analysis, Investigation, Visualization, Writing – review & editing.

Funding

This work was supported by Sichuan beef cattle innovation team of National Modern Agricultural Industry Technology System [SCCXTD-2024–13].

Disclosure statement

No potential conflict of interest was reported by the author(s).

Data availability statement

The chromosome-level genome assembly of *Trichophyton verrucosum* has been deposited in GenBank under accession number OR056436.1 (https://www.ncbi.nlm.nih.gov/nuccore/OR056436.1/). The raw sequence data reported in this study are available in the Genome Sequence Archive (GSA) at the National Genomics Data Center, China National Center for Bioinformation, Beijing Institute of Genomics, Chinese Academy of Sciences (https://ngdc.cncb.ac.cn/gsa), and can be accessed via Bio Project accession number PRJCA045930 https://ngdc.cncb.ac.cn/bioproject/browse/PRJCA045930.
The data supporting this study is available on 8 May 2025 under GSA accession number CRA029776. The data can be accessed through the following link: https://ngdc.cncb.ac.cn/gsa/browse/CRA029776. Supplementary materials, including figures and tables, can be accessed on Figshare at https://doi.org/10.6084/m9.figshare.31939248 [159], while the raw data are available on Figshare at https://doi.org/10.6084/m9.figshare.31939284 [160].

Ethical statement

Animal study was approved by the Sichuan Agricultural University Animal Ethics Committee (permit number 20220561). The study was conducted in compliance with local legislation and institutional requirements, ensuring ethical standards were upheld throughout the research process.

ORCID

Muhammad Salman Tahir http://orcid.org/0009-0009-5882-8437
Xiaoping Ma http://orcid.org/0000-0002-4950-8441
Yu Gu http://orcid.org/0000-0001-9086-8396

References

[1] Gupta C, Das S, Gaurav V, et al. Review on host-pathogen interaction in dermatophyte infections. J Med Mycology. 2023;33(1):101331. doi: 10.1016/j.mycmed.2022.101331
[2] Ivaskiene M, Matusevicius AP, Grigonis A, et al. Efficacy of topical therapy with newly developed terbinafine and econazole formulations in the treatment of dermatophytosis in cats. Pol J Vet Sci [Internet]. 2016 [cited 2025 Apr 30];19(3):535–543. doi: 10.1515/pjvs-2016-0067
[3] Indarjulianto S, Yanuartono Y, Widyarini S, et al. *Microsporum canis* infection in dermatitis cats Jurnal Veteriner. 2017 18 2 207–210 [cited 2025 Apr 30.
[4] Segal E, Elad D. Human and zoonotic dermatophytoses: epidemiological aspects. Front Microbiol. 2021;12:713532. doi: 10.3389/fmicb.2021.713532
[5] Moretti A, Agnetti F, Mancianti F, et al. Epidemiological, clinical and zoonotic aspects. G Ital Dermatol Venereol. 2013;148(6):563–572.
[6] Gnat S, Nowakiewicz A, Łagowski D, et al. Host-and pathogen-dependent susceptibility and predisposition to dermatophytosis. J Med Microbiol. 2019;68(6):823–836. doi: 10.1099/jmm.0.000982
[7] De Hoog S, Monod M, Dawson T, et al. Skin fungi from colonization to infection. In: Heitman J, BJ Howlett PW Crous, et al., editors. The fungal kingdom [Internet]. (WA) (DC), USA: ASM Press; 2017 [cited 2025 Jul 29]. p 855–871. doi: 10.1128/9781555819583.ch41
[8] Summerbell Rc WI, Summerbell RC. The dermatophytes. Clin Microbiol Rev. 1995;8(2):240–259. doi: 10.1128/CMR.8.2.240
[9] Wael F, Tayel AA, Mohamed RA, et al. Mixed rearing correlates with the existence of *trichophyton verrucosum* pathogens in humans [Internet]. Dermatologica Sinica: Elsevier; 2015 [cited 2025 Jul 28]. p. 130–133. Available from: ht tps://www.sciencedirect.com/science/article/pii/S1027811714000871
[10] De Hoog GS, Dukik K, Monod M, et al. Toward a novel multilocus phylogenetic taxonomy for the dermatophytes. Mycopathologia. 2017;182(1–2):5–31. doi: 10.1007/s11046-016-0073-9
[11] Persinoti GF, Martinez DA, Li W, et al. Whole-genome analysis illustrates global clonal population structure of the ubiquitous dermatophyte pathogen *trichophyton rubrum* [Internet]. Genetics. Oxford University Press; 2018 [cited 2025 Jul 28]. p. 1657–1669. Available from: https://academic.oup.com/genetics/article-abstract/208/4/1657/6084243
[12] Papini R, Nardoni S, Fanelli A, et al. High infection rate of *Trichophyton verrucosum* in calves from central Italy. Zoonoses Public Health. 2009;56(2):59–64. doi: 10.1111/j.1863-2378.2008.01157.x
[13] Hameed K, Ch FR, Nawaz MA, et al. *Trichophyton verrucosum* infection in livestock in the Chitral district of Pakistan [Internet]. The journal of infection in developing countries. 2017 [cited 2025 Jul 28]. p. 326–333. Available from: https://jidc.org/index.php/journal/article/view/7925
[14] Segal E, Elad D Human and zoonotic dermatophytoses: epidemiological aspects. Frontiers in Microbiology. ; 2021 12 []. p 713532.
[15] Chermette R, Ferreiro L, Guillot J. Dermatophytoses in animals. Mycopathologia [Internet]. 2008 [cited 2025 Jul 28];166(5–6):385–405. doi: 10.1007/s11046-008-9102-7
[16] Švarcová M, Větrovskỳ T, Kolařík M, et al. Defining the relationship between phylogeny, clinical manifestation, and phenotype for *trichophyton mentagrophytes/interdigitale* complex; a literature review and taxonomic recommendations [Internet]. Medical mycology. Oxford University Press; 2023 [cited 2025 Sept 2]. p.

myad042. Available from: https://academic.oup.com/mmy/article-abstract/61/5/myad042/7127701

[17] Courtellemont L, Chevrier S, Degeilh B, et al. Epidemiology of *trichophyton verrucosum* infection in Rennes University Hospital, France: a 12-year retrospective study [Internet]. Medical mycology. Oxford University Press; 2017 [cited 2025 Jul 28]. p. 720–724. Available from: https://academic.oup.com/mmy/article-abstract/55/7/720/2937965

[18] Gnat S, Łagowski D, Nowakiewicz A, et al. Infection of *Trichophyton verrucosum* in cattle breeders, Poland: a 40-year retrospective study on the genomic variability of strains. Mycoses [Internet]. 2018 [cited 2025 Jul 28];61(9):681–690. doi: 10.1111/myc.12791

[19] Neji S, Trabelsi H, Hadrich I, et al. Molecular characterization of strains of the *Trichophyton verrucosum* complex from Tunisia. Sabouraudia [Internet]. 2016 [cited 2025 Jul 28];54(8):787–793. doi: 10.1093/mmy/myw036

[20] Dalis JS, Kazeem HM, Kwaga JKP, et al. Prevalence and distribution of dermatophytosis lesions on cattle in Plateau State, Nigeria [Internet]. Veterinary world. 2019 [cited 2025 Jul 28]. p. 1484. Available from: https://pmc.ncbi.nlm.nih.gov/articles/PMC6813608/

[21] Dubljanin E, Džamić AM, Mitrović S, et al. Onychomycosis: clinical findings, etiological agents and evaluation of laboratory methods [Internet]. Archives of biological sciences. 2014 [cited 2025 Jul 28. p.587–594. ht tps://doiserbia.nb.rs/Article.aspx?id=0354-46641402587D.

[22] Johns LE, Goldman GH, Ries LN, et al. Nutrient sensing and acquisition in fungi: mechanisms promoting pathogenesis in plant and human hosts [Internet]. Fungal biology reviews. Elsevier. 2021 [cited 2025 Jul 28]. p. 1–14. Available from: https://www.sciencedirect.com/science/article/pii/S1749461321000026

[23] Muszewska A, Piłsyk S, Perlińska-Lenart U, et al. Diversity of cell wall related proteins in human pathogenic fungi [Internet]. Journal of Fungi. MDPI. 2017 [cited 2025 Sept 2]. p. 6. Available from: https://www.mdpi.com/2309-608X/4/1/6

[24] Beauvais A, Latgé J-P. Fungal cell wall [Internet]. Journal of Fungi. MDPI. 2018 [cited 2025 Sept 2]. p. 91. Available from: https://www.mdpi.com/2309-608X/4/3/91

[25] Tainwala R, Sharma YK. Pathogenesis of dermatophytoses [Internet]. Indian Journal of Dermatology. Medknow. 2011 [cited 2025 Jul 28]. p. 259–261. Available from: https://journals.lww.com/ijd/fulltext/2011/56030/pathogenesis_of_dermatophytoses.1.aspx

[26] Lopes L, Bitencourt TA, Lang EA, et al. Genes coding for LysM domains in the dermatophyte *Trichophyton rubrum*: a transcription analysis [Internet]. Medical mycology. Oxford University Press; 2020 [cited 2025 Jul 28]. p. 372–379. Available from: https://academic.oup.com/mmy/article-abstract/58/3/372/5521863

[27] Grumbt M, Monod M, Yamada T, et al. Keratin degradation by dermatophytes relies on cysteine dioxygenase and a sulfite efflux pump [Internet]. Journal of Investigative Dermatology. Elsevier. 2013 [cited 2025 Jul 28]. p. 1550–1555. Available from: https://www.sciencedirect.com/science/article/pii/S0022202X15362692

[28] Kasperova A, Kunert J, Raska M. The possible role of dermatophyte cysteine dioxygenase in keratin degradation [Internet]. Medical mycology. Informa UK Ltd UK; 2013 [cited 2025 Jul 28]. p. 449–454. Available from: https://academic.oup.com/mmy/article-abstract/51/5/449/951437

[29] Baldo A, Mathy A, Tabart J, et al. Secreted subtilisin Sub3 from *Microsporum canis* is required for adherence to but not for invasion of the epidermis [Internet]. British Journal of Dermatology. Oxford, (UK): Blackwell Publishing Ltd; 2010 [cited 2025 Jul 28]. p. 990–997. Available from: https://academic.oup.com/bjd/article-abstract/162/5/990/6642658

[30] de A PNT, da SLG, da S SR, et al. In vitro and ex vivo infection models help assess the molecular aspects of the interaction of *Trichophyton rubrum* with the host milieu. Sabouraudia [Internet]. 2016 [cited 2025 Jul 28];54(4):420–427.

[31] Goffeau A, Barrell BG, Bussey H, et al. Life with 6000 genes. Science [Internet]. 1996 [cited 2025 Jul 28];274(5287):546–567. doi: 10.1126/science.274.5287.546

[32] Burmester A, Shelest E, Glöckner G, et al. Comparative and functional genomics provide insights into the pathogenicity of dermatophytic fungi. Genome Biol [Internet]. 2011 [cited 2025 Jul 28];12(1):R7. doi: 10.1186/gb-2011-12-1-r7

[33] Martinez DA, Oliver BG, Gräser Y, et al. Berman J, editor. mBio [Internet]. Comparative genome analysis of *Trichophyton rubrum* and related dermatophytes reveals candidate genes involved in infection *m*Bio. 2012 [cited 2025 Jul 22];3(5). doi: 10.1128/mBio.00259-12

[34] Kar B, Patel P, Free SJ. *Trichophyton rubrum* LysM proteins bind to fungal cell wall chitin and to the N-linked oligosaccharides present on human skin glycoproteins [Internet]. PLOS ONE. San Francisco (CA) USA: Public Library of Science; 2019 [cited 2025 Jul 28]. p. e0215034. Available from: https://journals.plos.org/plosone/article?id=10.1371/journal.pone.0215034

[35] Liu L, Li Y, Li S, et al. Comparison of next-generation sequencing systems. J Biomed Biotechnol [Internet]. 2012 [cited 2025 Jul 28];2012:1–11. doi: 10.1155/2012/251364

[36] Rhoads A, Au KF. PacBio sequencing and its applications [Internet]. Genomics, proteomics & bioinformatics. Oxford University Press; 2015 [cited 2025 Jul 28]. p. 278–289. Available from: https://academic.oup.com/gpb/article-abstract/13/5/278/7224908

[37] Yang IS, Kim S. Analysis of whole transcriptome sequencing data: workflow and software [Internet]. Genomics & informatics. 2015 [cited 2025 Jul 22]. p. 119. Available from: https://pmc.ncbi.nlm.nih.gov/articles/PMC4742321/

[38] Sudhagar A, Kumar G, El-Matbouli M. Transcriptome analysis based on RNA-Seq in understanding pathogenic mechanisms of diseases and the immune system of fish: a comprehensive review. Int J Mol Sci [Internet]. 2018 [cited 2025 Jul 29];19(1):245. doi: 10.3390/ijms19010245

[39] Zhang H, He L, Cai L. Transcriptome sequencing: rNA-Seq. In: Huang T, editor. Computational systems biology [Internet]. New York (NY): Springer New York; 2018 [cited 2025 Jul 29]. p 15–27. Available from: https://doi.org/10.1007/978-1-4939-7717-8_2

[40] Wacker SA, Houghtaling BR, Elemento O, et al. Using transcriptome sequencing to identify mechanisms of drug action and resistance. Nat Chem Biol [Internet]. 2012 [cited 2025 Jul 29];8(3):235–237. doi: 10.1038/nchembio.779

[41] Xiao C-W, Ji Q-A, Wei Q, et al. Digital gene expression analysis of *microsporum canis* exposed to berberine chloride [Internet]. PLOS ONE. San Francisco (CA) USA: Public Library of Science; 2015 [cited 2025 Jul 22]. p. e0124265. Available from: https://journals.plos.org/plosone/article?id=10.1371/journal.pone.0124265

[42] Li Z, Qi F, Li F. Establishment of a gene signature to predict prognosis for patients with lung adenocarcinoma. Int J Mol Sci [Internet]. 2020 [cited 2025 Aug 1];21(22):8479. doi: 10.3390/ijms21228479

[43] Li M, Chen L, Zhao Y, et al. Research on the mechanism of HRP relieving IPEC-J2 cells immunological stress based on transcriptome sequencing analysis [Internet]. Frontiers in Nutrition. Frontiers Media SA. 2022 [cited 2025 Jul 22]. p. 944390. Available from: https://www.frontiersin.org/journals/nutrition/articles/10.3389/fnut.2022.944390/full

[44] Wang M, Zhao Y, Cao L, et al. Transcriptome sequencing revealed the inhibitory mechanism of ketoconazole on clinical *Microsporum canis*. J Vet Sci [Internet]. 2020 [cited 2025 Aug 1];22(1):e4.

[45] Persinoti GF, De Aguiar Peres NT, Jacob TR, et al. Rna-sequencing analysis of *Trichophyton rubrum* transcriptome in response to sublethal doses of acriflavine. BMC Genomics [Internet]. 2014 [cited 2025 Jul 29];15(S7):S1. doi: 10.1186/1471-2164-15-S7-S1

[46] Zhang X, Dai P, Gao Y, et al. Transcriptome sequencing and analysis of zinc-uptake-related genes in *Trichophyton mentagrophytes*. BMC Genomics [Internet]. 2017 [cited 2025 Jul 22];18(1). doi: 10.1186/s12864-017-4284-3

[47] Martins MP, Rossi A, Sanches PR, et al. Comprehensive analysis of the dermatophyte *Trichophyton rubrum* transcriptional profile reveals dynamic metabolic modulation [internet]. Biochemical journal. Portland Press Ltd.; 2020 [cited 2025 Jul 22]. p. 873–885. Available from: https://portlandpress.com/biochemj/article-abstract/477/5/873/222047

[48] Bok JW, Balajee SA, Marr KA, et al. Laea, a regulator of morphogenetic fungal virulence factors. Eukaryot Cell [Internet]. 2005 [cited 2025 Jul 28];4(9):1574–1582. doi: 10.1128/EC.4.9.1574-1582.2005

[49] Martinez-Rossi NM, Peres NTA, Rossi A. Pathogenesis of dermatophytosis: sensing the host tissue. Mycopathologia [Internet]. 2017 [cited 2025 Jul 28];182(1–2):215–227. doi: 10.1007/s11046-016-0057-9

[50] Cheng H, Jarvis ED, Fedrigo O, et al. Haplotype-resolved assembly of diploid genomes without parental data [Internet]. Nature Biotechnology. Nature Publishing Group US New York; 2022 [cited 2025 Jul 28]. p. 1332–1335. Available from: https://www.nature.com/articles/s41587-022-01261-x

[51] Simão FA, Waterhouse RM, Ioannidis P, et al. Busco: assessing genome assembly and annotation completeness with single-copy orthologs. Bioinformatics [Internet]. 2015 [cited 2024 Sept 26];31(19):3210–3212. doi: 10.1093/bioinformatics/btv351

[52] Rao SS, Huntley MH, Durand NC, et al. A 3D map of the human genome at kilobase resolution reveals principles of chromatin looping [Internet]. Cell Elsevier. 2014 159 7 [cited 2025 Jul 28]:1665–1680.

[53] Bolger AM, Lohse M, Usadel B. Trimmomatic: a flexible trimmer for Illumina sequence data [Internet]. Bioinformatics. Oxford University Press; 2014 [cited 2025 Jul 28]. p. 2114–2120. Available from: https://academic.oup.com/bioinformatics/article-abstract/30/15/2114/2390096

[54] Durand NC, Shamim MS, Machol I, et al. Juicer provides a one-click system for analyzing loop-resolution Hi-C experiments [Internet]. Cell systems. Elsevier. 2016 [cited 2025 Jul 28]. p. 95–98. Available from: https://www.cell.com/cell-systems/fulltext/S2405-4712(16)30219-8?code=cell-site&innerTabgraphical_S2405471216302198=

[55] Dudchenko O, Batra SS, Omer AD, et al. De novo assembly of the Aedes aegypti genome using Hi-C yields chromosome-length scaffolds [Internet]. Science. American Association for the Advancement of Science. 2017 [cited 2025 Jul 28]. p. 92–95. Available from: https://www.science.org/doi/abs/10.1126/science.aal3327

[56] Jurka JKapitonov VVPavlicek A *et al* Repbase update, a database of eukaryotic repetitive elementsCytogenetic and Genome Research. 2005. 1–4. 462–467.28Jul. Available from: https://karger.com/cgr/article-abstract/110/1-4/462/78195

[57] Open R. 4.0 2015 [http://www.repeatmasker.org]. Preprint at.

[58] Price AL, Jones NC, Pevzner PA. De novo identification of repeat families in large genomes [Internet]. Bioinformatics. Oxford University Press; 2005 [cited 2025 Jul 28]. p. i351–i358. Available from: https://www.academia.edu/download/49295669/RepeatDetection_Pevzner.pdf

[59] Xu Z, Wang H. Ltr_finder: an efficient tool for the prediction of full-length LTR retrotransposons [Internet]. Nucleic Acids Research. Oxford University Press; 2007 [cited 2025 Jul 28]. p. W265–W268. Available from: https://academic.oup.com/nar/article-abstract/35/suppl_2/W265/2920813

[60] Benson G. Tandem repeats finder: a program to analyze DNA sequences [Internet]. Nucleic Acids Research. Oxford University Press; 1999 [cited 2025 Jul 28]. p. 573–580. Available from: https://academic.oup.com/nar/article-abstract/27/2/573/1061099

[61] Lowe TM, Eddy SR. Trnascan-SE: a program for improved detection of transfer RNA genes in genomic sequence [Internet]. Nucleic Acids Research. Oxford University Press; 1997 [cited 2025 Jul 28]. p. 955–964. Available from: https://academic.oup.com/nar/article-abstract/25/5/955/5133591

[62] Lagesen K, Hallin P, Rødland EA, et al. Rnammer: consistent and rapid annotation of ribosomal RNA genes [Internet]. Nucleic Acids Research. Oxford University Press; 2007 [cited 2025 Jul 28]. p. 3100–3108. Available from: https://academic.oup.com/nar/article-abstract/35/9/3100/2401119

[63] Nawrocki EP, Kolbe DL, Eddy SR. Infernal 1.0: inference of RNA alignments [Internet]. Bioinformatics. Oxford University Press; 2009 [cited 2025 Jul 28]. p. 1335–1337. Available from: https://academic.oup.com/bioinformatics/article-abstract/25/10/1335/270663

[64] Kalvari I, Nawrocki EP, Ontiveros-Palacios N, et al. Rfam 14: expanded coverage of metagenomic, viral and microRNA families [internet]. Nucleic Acids Research. Oxford University Press; 2021 [cited 2025 Jul 28]. p. D192–D200. Available from: https://academic.oup.com/nar/article-abstract/49/D1/D192/5992291

[65] Gertz EM, Yu Y-K, Agarwala R, et al. Composition-based statistics and translated nucleotide searches: improving the tblastn module of BLAST. BMC Biol [Internet]. 2006 [cited 2025 Jul 28];4(1):41. doi: 10.1186/1741-7007-4-41

[66] Slater GSC, Birney E. Automated generation of heuristics for biological sequence comparison. BMC Bioinf [Internet]. 2005 [cited 2025 Jul 28];6(1):31. doi: 10.1186/1471-2105-6-31

[67] Trapnell C, Williams BA, Pertea G, et al. Transcript assembly and quantification by RNA-Seq reveals unannotated transcripts and isoform switching during cell differentiation [Internet]. Nature Biotechnology. Nature Publishing Group US New York; 2010 [cited 2025 Jul 28]. p. 511–515. Available from: https://www.nature.com/articles/nbt.1621

[68] Stanke M, Steinkamp R, Waack S, et al. Augustus: a web server for gene finding in eukaryotes [Internet]. Nucleic Acids Research. Oxford University Press; 2004 [cited 2025 Jul 28]. p. W309–W312. Available from: https://academic.oup.com/nar/article-abstract/32/suppl_2/W309/1040489

[69] Majoros WH, Pertea M, Salzberg SL. TigrScan and GlimmerHMM: two open source ab initio eukaryotic gene-finders [Internet]. Bioinformatics. Oxford University Press; 2004 [cited 2025 Jul 28]. p. 2878–2879. Available from: https://academic.oup.com/bioinformatics/article-abstract/20/16/2878/236797

[70] Burge C, Karlin S. Prediction of complete gene structures in human genomic DNA [Internet]. Journal of molecular biology. Elsevier. 1997 [cited 2025 Jul 28]. p. 78–94. Available from: https://www.sciencedirect.com/science/article/pii/S0022283697909517

[71] Cantarel BL, Korf I, Robb SM, et al. Maker: an easy-to-use annotation pipeline designed for emerging model organism genomes [Internet]. Genome research. Cold Spring Harbor Lab. 2008 [cited 2025 Jul 28]. p. 188–196. Available from: https://genome.cshlp.org/content/18/1/188.short

[72] Boeckmann B, Bairoch A, Apweiler R, et al. The Swiss-Prot protein knowledgebase and its supplement TrEMBL in 2003 [Internet]. Nucleic Acids Research. Oxford University Press; 2003 [cited 2025 Jul 28]. p. 365–370. Available from: https://academic.oup.com/nar/article-abstract/31/1/365/2401437

[73] Ashburner M, Ball CA, Blake JA, et al. Gene ontology: tool for the unification of biology [Internet]. Nature genetics. Nature Publishing Group; 2000 [cited 2025 Jul 28]. p. 25–29. Available from: https://www.nature.com/articles/ng0500_25

[74] Kanehisa M, Goto S, Sato Y, et al. Kegg for integration and interpretation of large-scale molecular data sets [Internet]. Nucleic acids research. Oxford University Press; 2012 [cited 2025 Jul 28]. p. D109–D114. Available from: https://academic.oup.com/nar/article-abstract/40/D1/D109/2903713

[75] Mitchell A, Chang H-Y, Daugherty L, et al. The InterPro protein families database: the classification resource after 15 years [Internet]. Nucleic Acids Research. Oxford University Press; 2015 [cited 2025 Jul 28]. p. D213–D221. Available from: https://academic.oup.com/nar/article-abstract/43/D1/D213/2439465

[76] Huang F, Fu M, Li J, et al. Analysis and prediction of protein stability based on interaction network, gene ontology, and KEGG pathway enrichment scores [Internet]. Biochimica et Biophysica Acta (BBA)-proteins and proteomics. Elsevier. 2023 [cited 2025 Jul 28]. p. 140889. Available from: https://www.sciencedirect.com/science/article/pii/S157096392300002X

[77] Snow M, Jermain P, Mandalia V, et al. A 2021 consensus statement on osteotomies around the knee by the UK Knee Osteotomy Consensus Group (KOG). Knee [Internet]. 2021 [cited 2025 Jul 29];33:73–83. doi: 10.1016/j.knee.2021.08.034

[78] Blin K, Shaw S, Kloosterman AM, et al. AntiSMASH 6.0: improving cluster detection and comparison capabilities [Internet]. Nucleic Acids Research. Oxford University Press; 2021 [cited 2025 Jul 28]. p. W29–W35. Available from: https://academic.oup.com/nar/article-abstract/49/W1/W29/6274535

[79] Lombard V, Golaconda Ramulu H, Drula E, et al. The carbohydrate-active enzymes database (CAZy) in 2013 [Internet]. Nucleic acids research. Oxford University Press; 2014 [cited 2025 Jul 28]. p. D490–D495. Available from: https://academic.oup.com/nar/article-abstract/42/D1/D490/1057423

[80] Zhang H, Yohe T, Huang L, et al. DbCAN2: a meta server for automated carbohydrate-active enzyme annotation [Internet]. Nucleic Acids Research. Oxford University Press; 2018 [cited 2025 Jul 28]. p. W95–W101. Available from: https://academic.oup.com/nar/article-abstract/46/W1/W95/4996582

[81] Winnenburg R, Baldwin TK, Urban M, et al. Phi-base: a new database for pathogen host interactions [Internet]. Nucleic Acids Research. Oxford University Press; 2006 [cited 2025 Jul 28]. p. D459–D464. Available from: https://academic.oup.com/nar/article-abstract/34/suppl_1/D459/1132790

[82] Lu T, Yao B, Zhang C. Dfvf: database of fungal virulence factors [Internet]. Database. Oxford Academic; 2012 [cited 2025 Jul 28]. Available from: https://academic.oup.com/database/article/doi/10.1093/database/bas032/436515?ijkey=5IyN2HrtlNrJpzz&keytype=ref

[83] Emms DM, Kelly S. Orthofinder: phylogenetic orthology inference for comparative genomics. Genome Biol [Internet]. 2019 [cited 2025 Jul 28];20(1):238. doi: 10.1186/s13059-019-1832-y

[84] Katoh K, Standley DM. Mafft multiple sequence alignment software version 7: improvements in performance and usability. Mol Biol Evol. 2013;30(4):772–780. doi: 10.1093/molbev/mst010

[85] Nguyen L-T, Schmidt HA, Von Haeseler A, et al. Iq-tree: a fast and effective stochastic algorithm for estimating maximum-likelihood phylogenies [Internet]. Molecular biology and evolution. Oxford University Press; 2015 [cited 2025 Jul 28]. p. 268–274. Available from: https://academic.oup.com/mbe/article-abstract/32/1/268/2925592

[86] Wang Y, Tang H, DeBarry JD, et al. Mcscanx: a toolkit for detection and evolutionary analysis of gene synteny and collinearity [internet]. Nucleic Acids Research. Oxford University Press; 2012 [cited 2025 Jul 28]. p. e49–e49. Available from: https://academic.oup.com/nar/article-abstract/40/7/e49/1202057

[87] Kim D, Langmead B, Salzberg SL. Hisat: a fast spliced aligner with low memory requirements [Internet]. Nature methods. Nature Publishing Group US New York; 2015 [cited 2025 Jul 28]. p. 357–360. Available from: https://www.nature.com/articles/nmeth.3317

[88] Kim D, Paggi JM, Park C, et al. Graph-based genome alignment and genotyping with HISAT2 and HISAT-genotype [Internet]. Nature biotechnology. Nature Publishing Group US New York; 2019 [cited 2025 Jul 28]. p. 907–915. Available from: https://www.nature.com/articles/s41587-019-0201-4

[89] Pertea M, Pertea GM, Antonescu CM, et al. StringTie enables improved reconstruction of a transcriptome from RNA-seq reads [Internet]. Nature biotechnology. Nature Publishing Group; 2015 [cited 2025 Jul 28]. p. 290–295. Available from: https://www.nature.com/articles/nbt.3122.pdf

[90] Pertea M, Kim D, Pertea GM, et al. Transcript-level expression analysis of RNA-seq experiments with HISAT, StringTie and ballgown [Internet]. Nature protocols. Nature Publishing Group UK London; 2016 [cited 2025 Jul 28]. p. 1650–1667. Available from: https://www.nature.com/articles/nprot.2016.095

[91] Love MI, Huber W, Anders S. Moderated estimation of fold change and dispersion for RNA-seq data with DESeq2. Genome Biol [Internet]. 2014 [cited 2025 Jul 28];15(12):550. doi: 10.1186/s13059-014-0550-8

[92] Kanehisa M, Furumichi M, Sato Y, et al. Kegg: integrating viruses and cellular organisms [Internet]. Nucleic Acids Research. Oxford University Press; 2021 [cited 2025 Jul 28]. p. D545–D551. Available from: https://academic.oup.com/nar/article-abstract/49/D1/D545/5943834

[93] Livak KJ, Schmittgen TD. Analysis of relative gene expression data using real-time quantitative PCR and the 2- δδct method [Internet]. Methods. Elsevier. 2001 [cited 2025 Jul 28]. p. 402–408. Available from: https://www.sciencedirect.com/science/article/pii/S1046202301912629

[94] Subramanian A, Tamayo P, Mootha VK, et al. Gene set enrichment analysis: a knowledge-based approach for interpreting genome-wide expression profiles. Proc Natl Acad Sci USA [Internet]. 2005 [cited 2025 Jul 28];102(43):15545–15550. doi: 10.1073/pnas.0506580102

[95] Agnetti F, Righi C, Scoccia E, et al. *Trichophyton verrucosum* infection in cattle farms of Umbria (central Italy) and transmission to humans. Mycoses [Internet]. 2014 [cited 2025 Jul 28];57(7):400–405. doi: 10.1111/myc.12174

[96] Dalis JS, Kazeem HM, Kwaga JK, et al. Molecular characterization of dermatophytes isolated from cattle in Plateau State, Nigeria [Internet]. Veterinary microbiology. Elsevier. 2018 [cited 2025 Jul 28]. p. 212–218. Available from: https://www.sciencedirect.com/science/article/pii/S0378113517307368

[97] Ming PX, Ylx T, Bulmer GS. Outbreak of *Trichophyton verrucosum* in China transmitted from cows to humans. Mycopathologia [Internet]. 2006 [cited 2025 Jul 28];161(4):225–228.

[98] Taylor JW, Berbee ML. 1 fungi from PCR to genomics: the spreading revolution in evolutionary biology. In: McLaughlin DJ JW Spatafora, editors. Systematics and evolution [Internet]. Berlin, Heidelberg: Springer Berlin Heidelberg; 2014 [cited 2025 Jul 28]. p 1–18. https://link.springer.com/10.1007/978-3-642-55318-9.

[99] Fitzpatrick D. Fungal genomics. In: Kavanagh K, editor. Fungi: Biology and Applications 3rd ed. (Chichester, UK: Wiley). 2017 [cited 2025 Jul 28]. p 67–89. Available from: https://onlinelibrary.wiley.com/doi/10.1002/9781119374312.ch3

[100] Land M, Hauser L, Jun S-R, et al. Insights from 20 years of bacterial genome sequencing. Funct Integr Genomics [Internet]. 2015 [cited 2025 Jul 28];15(2):141–161. doi: 10.1007/s10142-015-0433-4

[101] Chin C-S, Sorenson J, Harris JB, et al. The origin of the Haitian cholera outbreak strain. N Engl J Med [Internet]. 2011 [cited 2025 Jul 28];364(1):33–42. doi: 10.1056/NEJMoa1012928

[102] Liu W, Shi X, Cai Y, et al. Two near-chromosomal-level genomes of globally-distributed macroascomycete based on single-molecule fluorescence and Hi-C methods [Internet]. Scientific Data. Nature Publishing Group UK London; 2024 [cited 2025 Jul 28]. p. 964. Available from: https://www.nature.com/articles/s41597-024-03794-z

[103] Faino L, Seidl MF, Datema E, et al. Kaemper J, Kahmann R, editors. mBio [Internet]. Single-molecule real-time sequencing combined with optical mapping yields completely finished fungal genome *m*Bio. 2015 [cited 2025 Jul 28];6(4):e00936–15. doi: 10.1128/mBio.00936-15

[104] Ge L, Liu J, Zheng H, et al. Comprehensive genome and transcriptome analysis of the dermatophyte *Trichophyton schoenleinii* reveals the candidate pathogenic genes. Mycoses [Internet]. 2021 [cited 2025 Jul 28];64(6):624–633. doi: 10.1111/myc.13257

[105] Zheng H, Blechert O, Mei H, et al. Assembly and analysis of the whole genome of *Arthroderma uncinatum* strain T10, compared with *Microsporum canis* and

Trichophyton rubrum. Mycoses [Internet]. 2020 [cited 2025 Jul 28];63(7):683–693. doi: 10.1111/myc.13079

[106] Granados-Casas AO, Sastoque AP, Stchigel AM, et al. Hybrid de novo whole-genome assembly, annotation, and identification of secondary metabolite gene clusters in the ex-type strain of *Chrysosporium keratinophilum* [Internet]. J of fungi. MDPI; 2023. [cited 2025 Jul 28]. p. 389. Available from: https://www.mdpi.com/2309-608X/9/4/389

[107] Granados-Casas AO, Fernández-Bravo A, Stchigel AM, et al. Genomic sequencing and functional analysis of the ex-type strain of *Malbranchea zuffiana* [Internet]. J of fungi. MDPI; 2024. [cited 2025 Jul 28]. p. 600. Available from: https://www.mdpi.com/2309-608X/10/9/600

[108] Feng S, Wang Z, Lin K, et al. Haplotype-resolved genomes of *trichophyton mentagrophytes* and *trichophyton tonsurans* [Internet]. Scientific Data. Nature Publishing Group UK London; 2025 [cited 2025 Jul 28]. p. 559. Available from: https://www.nature.com/articles/s41597-025-04835-x

[109] Li S-F, Gao W-J, Zhao X-P, et al. Analysis of transposable elements in the genome of *asparagus officinalis* from high coverage sequence data [Internet]. PLOS ONE. San Francisco (USA): Public Library of Science; 2014 [cited 2025 Jul 28]. p. e97189. Available from: https://journals.plos.org/plosone/article?id=10.1371/journal.pone.0097189

[110] Daboussi M-J, Capy P. Transposable elements in filamentous fungi. Annu Rev Microbiol [Internet]. 2003 [cited 2025 Jul 28];57(1):275–299. doi: 10.1146/annurev.micro.57.030502.091029

[111] Lorrain C, Feurtey A, Möller M, et al. Dynamics of transposable elements in recently diverged fungal pathogens: lineage-specific transposable element content and efficiency of genome defenses. G3 [Internet]. 2021 [cited 2025 Jul 28];11(4):jkab068. doi: 10.1093/g3journal/jkab068

[112] Fouché S, Plissonneau C, Croll D. The birth and death of effectors in rapidly evolving filamentous pathogen genomes. Curr Opin Microbiol [Internet]. 2018 [cited 2025 May 19];46:34–42. doi: 10.1016/j.mib.2018.01.020

[113] Fokkens L, Shahi S, Connolly LR, et al. The multi-speed genome of *Fusarium oxysporum* reveals association of histone modifications with sequence divergence and footprints of past horizontal chromosome transfer events. bioRxiv [Internet]. 2018 [cited 2025 May 19]; p. 465070.

[114] Galagan JE, Calvo SE, Borkovich KA, et al. The genome sequence of the filamentous fungus Neurospora crassa [Internet]. Nature. Nature Publishing Group UK London; 2003 [cited 2025 Jul 28]. p. 859–868. Available from: https://www.nature.com/articles/nature01554

[115] Cuomo CA, Güldener U, Xu J-R, et al. The *Fusarium graminearum* genome reveals a link between localized polymorphism and pathogen specialization. Science [Internet]. 2007 [cited 2025 Jul 28];317(5843):1400–1402. doi: 10.1126/science.1143708

[116] Kubicek CP, Herrera-Estrella A, Seidl-Seiboth V, et al. Comparative genome sequence analysis underscores mycoparasitism as the ancestral lifestyle of *Trichoderma*. Genome Biol [Internet]. 2011 [cited 2025 Jul 28];12(4):R40. doi: 10.1186/gb-2011-12-4-r40

[117] Desjardins CA, Champion MD, Holder JW, et al. Comparative genomic analysis of human fungal pathogens causing paracoccidioidomycosis [Internet].Plos genetics San Francisco (USA): Public Library of Science; 2011 [cited 2025 Jul 28]. p. e1002345. Available from: https://journals.plos.org/plosgenetics/article?id=10.1371/journal.pgen.1002345

[118] Keller NP. Fungal secondary metabolism: regulation, function and drug discovery [Internet]. Nature Reviews Microbiology. Nature Publishing Group UK London; 2019 [cited 2025 Jul 28]. p. 167–180. Available from: https://www.nature.com/articles/s41579-018-0121-1

[119] Li C, Pang A-P, Yang H, et al. Tracking localization and secretion of cellulase spatiotemporally and directly in living *Trichoderma reesei*. Biotechnol Biofuels [Internet]. 2019 [cited 2025 Jul 28];12(1):200. doi: 10.1186/s13068-019-1538-0

[120] Zhang T, Liu H, Lv B, et al. Regulating strategies for producing carbohydrate active enzymes by filamentous fungal cell factories. Front Bioeng Biotechnol [Internet]. 2020 [cited 2025 Jul 28];8:691. doi: 10.3389/fbioe.2020.00691

[121] Park BH, Karpinets TV, Syed MH, et al. Cazymes analysis toolkit (CAT): web service for searching and analyzing carbohydrate-active enzymes in a newly sequenced organism using CAZy database. Glycobiology [Internet]. 2010 [cited 2025 Jul 28];20(12):1574–1584. doi: 10.1093/glycob/cwq106

[122] Salam LB. Detection of carbohydrate-active enzymes and genes in a spent engine oil-perturbed agricultural soil. Bull Natl Res Cent [Internet]. 2018 [cited 2025 Jul 28];42(1):10. doi: 10.1186/s42269-018-0013-6

[123] Rafiei V, Vélëz H, Tzelepis G. The role of glycoside hydrolases in phytopathogenic fungi and oomycetes virulence [Internet]. International journal of molecular sciences. MDPI. 2021 [cited 2025 Jul 28]. p. 9359. Available from: https://www.mdpi.com/1422-0067/22/17/9359

[124] Park Y-J, Jeong Y-U, Kong W-S. Genome sequencing and carbohydrate-active enzyme (CAZyme) repertoire of the white rot fungus *Flammulina elastica* [Internet]. International journal of molecular sciences. MDPI; 2018. [cited 2025 Jul 28]. p. 2379. Available from: https://www.mdpi.com/1422-0067/19/8/2379

[125] Deng Q, Wu H, Gu Q, et al. Glycosyltransferase FvCpsA regulates fumonisin biosynthesis and virulence in *Fusarium verticillioides* [Internet]. Toxins. MDPI; 2021 [cited 2025 Jul 28]. p. 718. Available from: https://www.mdpi.com/2072-6651/13/10/718

[126] Urban M, Cuzick A, Seager J, et al. Phi-base: the pathogen–host interactions database [internet]. Nucleic acids research. Oxford University Press; 2020 [cited 2025 Jul 28]. p. D613–D620. Available from: https://academic.oup.com/nar/article-abstract/48/D1/D613/5626528

[127] Nielsen H. Predicting secretory proteins with SignalP. In: Kihara D, editor. Protein function prediction [Internet]. New York (NY): Springer New York; 2017 [cited 2025 Jul 28]. p 59–73. Available from: https://doi.org/10.1007/978-1-4939-7015-5_6

[128] Zhan P, Dukik K, Li D, et al. Phylogeny of dermatophytes with genomic character evaluation of clinically distinct *Trichophyton rubrum* and *T. violaceum* [internet]. Studies in mycology. Westerdijk Fungal Biodiversity Institute; 2018. [cited 2025 Jul 28]. p. 153–175. Available from: https://www.ingentaconnect.com/content/wfbi/sim/2018/00000089/00000001/art00011

[129] Kaplan E, Gonca S, Kandemir H, et al. Genes encoding proteolytic enzymes fungalysin and subtilisin in dermatophytes of human and animal origin: a comparative study. Mycopathologia [Internet]. 2019 [cited 2025 Jul 28]. doi: 10.1007/s11046-019-00367-2

[130] Mercer DK, Stewart CS. Keratin hydrolysis by dermatophytes [Internet]. Medical mycology. Oxford University Press; 2019 [cited 2025 Sept 2]. p. 13–22. Available from: https://academic.oup.com/mmy/article-abstract/57/1/13/4816029

[131] Khedmati E, Hazaveh SJH, Bayat M, et al. Identification of subtilisin virulence genes (SUB1-7) in *Epidermophyton floccosum* isolated from patients with dermatophytosis in Iran [Internet]. Gene reports. Elsevier; 2020 [cited 2025 Sept 2]. p.100748. Available from: https://www.sciencedirect.com/science/article/pii/S245201442030162X

[132] Baumbach C, Michler JK, Nenoff P, et al. Visualising virulence factors: *Trichophyton benhamiaes* subtilisins demonstrated in a guinea pig skin ex vivo model. Mycoses [Internet]. 2020 [cited 2025 May 19];63(9):970–978. doi: 10.1111/myc.13136

[133] Naeimipour F, Hashemi SJ, Rezaie S, et al. Subtilisin gene activity in dermatophytes: a study on the presence of the subtilisin gene in *Trichophyton verrucosum* and *Microsporum gypseum* in clinical and nonclinical samples in Tehran, Iran. Arch Razi Inst [Internet]. 2021 [cited 2025 May 19];76(2):253.

[134] Vite-Garín T, Estrada-Cruz NA, Hernández-Castro R, et al. Remarkable phenotypic virulence factors of *Microsporum canis* and their associated genes: a systematic review. Int J Mol Sci [Internet]. 2024 [cited 2025 May 19];25(5):2533. doi: 10.3390/ijms25052533

[135] Chen J, Yi J, Liu L, et al. Substrate adaptation of *Trichophyton rubrum* secreted endoproteases [Internet]. Microbial pathogenesis. Elsevier; 2010. [cited 2025 Jul 28]. p. 57–61. Available from: https://www.sciencedirect.com/science/article/pii/S0882401009002010

[136] Staib P, Zaugg C, Mignon B, et al. Differential gene expression in the pathogenic dermatophyte *Arthroderma benhamiae* in vitro versus during infection. Microbiology [Internet]. 2010 [cited 2025 Jul 28];156(3):884–895. doi: 10.1099/mic.0.033464-0

[137] Łagowski D, Gnat S, Nowakiewicz A, et al. Comparison of in vitro activities of 11 antifungal agents against *Trichophyton verrucosum* isolates associated with a variety hosts and geographical origin. Mycoses [Internet]. 2020 [cited 2025 May 18];63(3):294–301. doi: 10.1111/myc.13042

[138] Kaplan E, Gonca S, Kandemir H, et al. Genes encoding proteolytic enzymes fungalysin and subtilisin in dermatophytes of human and animal origin: a comparative study. Mycopathologia [Internet]. 2019 [cited 2025 May 19]. doi: 10.1007/s11046-019-00367-2

[139] Khalili M, Bayat M, Hazaveh SJH, et al. Subtilisin genes (SUB1-3) presence in *Microsporum canis* isolates with human and animal source. Research in molecular medicine (RMM) [Internet]. 2018. [cited 2025 May 19]. p. 54–62.

[140] Liu J, Ge L, Mei H, et al. Comparative genomics and molecular analysis of Epidermophyton floccosum. Mycopathologia [Internet]. 2021 [cited 2025 Jul 28];186(4):487–497. doi: 10.1007/s11046-021-00567-9

[141] Martinez-Rossi NM, Peres NTA, Rossi A. Antifungal resistance mechanisms in dermatophytes. Mycopathologia [Internet]. 2008 [cited 2025 Jul 29];166(5–6):369–383. doi: 10.1007/s11046-008-9110-7

[142] Costa C, Dias PJ, Sá-Correia I, et al. MFS multidrug transporters in pathogenic fungi: do they have real clinical impact? Front Physiol [Internet]. 2014 [cited 2025 Jul 29];5:197.

[143] Scorzoni L, de Paulae, Silva AC, et al. Antifungal therapy: new advances in the understanding and treatment of mycosis. Front Microbiol [Internet]. 2017 [cited 2025 Jul 29];8:36.

[144] Fachin AL, Ferreira-Nozawa MS, Maccheroni W, et al. Role of the ABC transporter TruMDR2 in terbinafine, 4-nitroquinoline N-oxide and ethidium bromide susceptibility in *Trichophyton rubrum*. J Med Microbiol [Internet]. 2006 [cited 2025 Jul 29];55(8):1093–1099. doi: 10.1099/jmm.0.46522-0

[145] Maranhão FCA, Paião FG, Fachin AL, et al. Membrane transporter proteins are involved in *Trichophyton rubrum* pathogenesis. J Med Microbiol [Internet]. 2009 [cited 2025 Sept 2];58(2):163–168. doi: 10.1099/jmm.0.002907-0

[146] Lamb DC, Waterman MR, Kelly SL, et al. Cytochromes P450 and drug discovery. Curr Opin Biotechnol [Internet]. 2007 [cited 2025 Jul 29];18(6):504–512. doi: 10.1016/j.copbio.2007.09.010

[147] Zhang J, Li L, Lv Q, et al. The fungal CYP51s: their functions, structures, related drug resistance, and inhibitors. Front Microbiol [Internet]. 2019 [cited 2025 Jul 29];10:691. doi: 10.3389/fmicb.2019.00691

[148] Yun Y, Yin D, Dawood DH, et al. Functional characterization of FgERG3 and FgERG5 associated with ergosterol biosynthesis, vegetative differentiation and virulence of *Fusarium graminearum*. Fungal Genet Biol [Internet]. 2014 [cited 2025 Jul 29];68:60–70. doi: 10.1016/j.fgb.2014.04.010

[149] Khan R, Tan R, Mariscal AG, et al. A binuclear zinc transcription factor binds the host isoflavonoid-responsive element in a fungal cytochrome P450 gene responsible for detoxification. Mol Microbiol [Internet]. 2003 [cited 2025 Jul 28];49(1):117–130. doi: 10.1046/j.1365-2958.2003.03552.x

[150] Kagan IA, Michel A, Prause A, et al. Gene transcription profiles of *Saccharomyces cerevisiae* after treatment with plant protection fungicides that inhibit ergosterol biosynthesis. Pestic Biochem Physiol [Internet]. 2005 [cited 2025 Jul 29];82(2):133–153. doi: 10.1016/j.pestbp.2005.02.002

[151] Becher R, Wirsel SGR. Fungal cytochrome P450 sterol 14α-demethylase (CYP51) and azole resistance in plant

and human pathogens. Appl Microbiol Biotechnol [Internet]. 2012 [cited 2025 Jul 28];95(4):825–840. doi: 10.1007/s00253-012-4195-9

[152] Zhang W, Yu L, Yang J, et al. Transcriptional profiles of response to terbinafine in *Trichophyton rubrum*. Appl Microbiol Biotechnol [Internet]. 2009 [cited 2025 Jul 28];82(6):1123–1130. doi: 10.1007/s00253-009-1908-9

[153] Hong JS, Lee DW, Suh MK, et al. Macroscopic and microscopic findings of *Trichophyton verrucosum* isolated from cattle. J Mycol Infect [Internet]. 2018 [cited 2025 Jul 28];25(2):89–96.

[154] Kane J. Early detection and identification of *Trichophyton verrucosum*. J Clin Microbiol. 1978 [cited 2025 Jul 28];7(3):194–196.

[155] Kosuge J, Goto Y, Shinjo T, et al. The influence of urea, ammonia. Jpn J Med Mycol. 2002 [cited 2025 Jul 28];43(2):99–102. doi: 10.3314/jjmm.43.99

[156] Kim SJ. Mycological features of *Trichophyton verrucosum* isolated in cattle. BSL. 2019 [cited 2025 Jul 28];25(4):367–371. doi: 10.15616/BSL.2019.25.4.367

[157] Spanamberg A, Ravazzolo AP, Araujo R, et al. Bovine ringworm: detection of *Trichophyton verrucosum* by SYBR-Green real-time PCR. Med Mycol Case Rep. 2023 [cited 2025 Jul 28];22(1):45–50.

[158] Łagowski D, Gnat S, Nowakiewicz A, et al. Real-time PCR as an alternative technique for detection of dermatophytes in cattle and environment. Med Mycol. 2021 [cited 2025 Jul 28];59(3):240–245.

[159] Tahir MS. Chromosome-level genome and transcriptome analysis of *Trichophyton verrucosum* reveals pathogenicity mechanisms and antifungal response [Internet]. 2026 [cited 2026 May 8]. Available from: https://figshare.com/articles/dataset/Supplementary_Figures_and_Tables/31939248/2

[160] Tahir MS. Chromosome-level genome and transcriptome analysis of *Trichophyton verrucosum* reveals pathogenicity mechanisms and antifungal response [Internet]. 2026 [cited 2026 May 8]. Available from: https://figshare.com/articles/dataset/qPCR_Gene_Validation_Data_and_Database_Results_for_Phi_Cazy_and_Dfvf_Genes_Comparative_Expression_Analysis/31939284/2